ECM-mimicking hydrogel models of human adipose tissue identify deregulated lipid metabolism in the prostate cancer-adipocyte crosstalk under antiandrogen therapy

Agathe Bessot [a,b,c,d], Joan Röhl [e,1], Maria Emmerich [f,1], Anton Klotz [g,1],
Akhilandeshwari Ravichandran [b,h,i,1], Christoph Meinert [j,1], David Waugh [k,1],
Jacqui McGovern [a,b,c,i], Jenni Gunter [a,d], Nathalie Bock [a,b,c,d,l,*]

[a] School of Biomedical Sciences, Faculty of Health, and Translational Research Institute (TRI), Queensland University of Technology (QUT), Brisbane, QLD, 4102, Australia
[b] Centre for Biomedical Technologies, QUT, Brisbane, QLD, 4000, Australia
[c] Max Planck Queensland Centre, Brisbane, QLD, 4000, Australia
[d] Australian Prostate Cancer Research Centre (APCRC-Q), QUT, Brisbane, QLD, 4102, Australia
[e] Faculty of Health Sciences and Medicine, Bond University, Robina, QLD, 4226, Australia
[f] School of Computation, Information and Technology, Technical University of Munich (TUM), Munich, Germany
[g] Division of Gastroenterology and Hepatology, Department of Internal Medicine 3, Medical University of Vienna, Vienna, Austria
[h] School of Mechanical, Medical and Process Engineering, Faculty of Engineering, QUT, Brisbane, QLD 4000, Australia
[i] Australian Research Council (ARC) Training Centre for Cell and Tissue Engineering Technologies (CTET), QUT, Brisbane, QLD 4000, Australia
[j] Gelomics Pty Ltd., Brisbane, QLD 4059, Australia
[k] Centre for Cancer Biology, University of South Australia, Adelaide, SA 5005, Australia
[l] Australian Research Council (ARC) Training Centre for Multiscale 3D Imaging, Modelling, and Manufacturing (M3D Innovation), Queensland University of Technology, Brisbane, QLD 4000, Australia

ARTICLE INFO

ABSTRACT

Antiandrogen therapies are effectively used to treat advanced prostate cancer, but eventually cancer adaptation drives unresolved metastatic castration-resistant prostate cancer (mCRPC). Adipose tissue influences metabolic reprogramming in cancer and was proposed as a contributor to therapy resistance. Using extracellular matrix (ECM)-mimicking hydrogel coculture models of human adipocytes and prostate cancer cells, we show that adipocytes from subcutaneous or bone marrow fat have dissimilar responses under the antiandrogen Enzalutamide. We demonstrate that androgen receptor (AR)-dependent cancer cells (LNCaP) are more influenced by human adipocytes than AR-independent cells (C4-2B), with altered lipid metabolism and adipokine secretion. This response changes under Enzalutamide, with increased AR expression and adipogenic and lipogenic genes in cancer cells and decreased lipid content and gene dysregulation associated with insulin resistance in adipocytes. This is in line with the metabolic syndrome that men with mCRPC under Enzalutamide experience. The all-human, all-3D, models presented here provide a significant advance to dissect the role of fat in therapy response for mCRPC.

1. Introduction

Metabolic reprogramming is one of the key hallmarks in cancer [1], with profound effects on gene expression, cellular differentiation, and the tumor microenvironment [2]. Cancer-associated metabolic events include deregulated uptake of glucose and amino acids, the use of glycolysis/tricarboxylic acid (TCA) cycle intermediates for biosynthesis and essential nicotinamide adenine dinucleotide phosphate (NADPH) production, and alterations in metabolite-driven gene regulation [3]. These adaptations enable rapidly proliferating cancer cells to sustain their high energetic and biosynthesis needs. With a clear link between metabolism and cancer [1–3], and adipocytes being a major source of

energy and key regulator of metabolism [4], studies of the cancer cell-adipocyte crosstalk have long established the risk between obesity and cancer [5]. In obesity, the dysregulation of adipose tissue composition, including adipocyte hyperplasia and hypertrophy, creates a proinflammatory milieu supportive of tumor growth, shown to provide a moderate risk increase (1.5–2.99 fold) for liver, pancreas and kidney cancers and high risk increase (3+ fold) for esophagus and uterus cancers [6].

In prostate cancer (PCa), the periprostatic adipose tissue contribution includes the insulin and insulin-like growth factor (IGF)-1 axis, fatty acid-binding protein 4 (FABP4), sex steroids, and adipokines, helping dissemination past the prostate [7]. Due to a permissive premetastatic niche enriched with a high variety of cytokines and growth factors, bone is a common secondary site in advanced PCa [8]. In this microenvironment, bone marrow adipose tissue (BMAT) comprises over 70 % of the bone marrow in adults. Yet, bone marrow adipocytes (BMAs) are fundamentally different from the white adipocytes (WAs) found in the primary PCa niche [9] and other subcutaneous and visceral adipose depots, known as white adipose tissue (WAT). While similarities between BMAs and WAs include being composed of neutral lipids, storing and releasing free fatty acids (FFAs), differences include a profound lipolysis deficiency in BMAs, due to Monoglyceride Lipase (MGLL) downregulation. Instead, BMAs exhibit a cholesterol-oriented metabolism with increased free cholesterol content, and have decreased insulin responsiveness [10]. These differences make it difficult to deconvolute the various cell and tissue contributions to disease and call for a larger variety of adipocyte models.

Despite a strong focus on the role of WAT in cancer, the specific role of BMAT in bone cancer metastasis is not understood partly due to difficulties in accessing this niche. Yet, it has already been reported that adipocyte-induced inflammation is linked with skeletal metastases [11]. Adipocytes found in proximity to cancer cells display reduced cell size, smaller lipid droplets and dysregulated phenotypes, identified as cancer-associated BMAs (CA-BMAs). CA-BMAs enhance cancer progression within the bone microenvironment via prosurvival factors, such as STAT3, Akt and MAPK signaling, through a proinflammatory profile expression of IL-6, IL-1β, CXCL1/2 and leptin and the downregulation of antitumor factors (i.e., adiponectin), promoting the metastatic process in the bone niche overexpression [12,13]. Cancer cells also induce FFA release from BMAs and develop storage capability via CD36 and FABP4, as an energy source. In addition to fueling cancer cells, CA-BMAs also modulate the bone microenvironment. They inhibit osteoblast differentiation (blocking BMP-signaling and activating NF-κB) [14] and promote osteoclast formation [15] and differentiation [16], to promote cancer progression, as reported for breast and lung cancer bone metastasis [17,18]. CA-BMAs also provide cancer cell survival benefits against therapies, with leptin a central contributor to chemotherapy and radiotherapy resistance via TGF-β, JAK/STAT, PI3K, HIF, and MAPK pathways [17], and by sequestering chemotherapies within their lipid droplets [19].

In prostate cancer in bone, resistance to Docetaxel was demonstrated by the enhanced activity of IL-1β/COX-2/MCP-1 axis and a resulting increase in PGE$_2$ production by adipocytes, concurring with augmented hypoxia signaling and activation of prosurvival pathways in tumor cells [20]. Enzalutamide, a nonsteroidal second-generation antiandrogen, is highly efficient initially for PCa, blocking castration-resistant prostate cancer (CRPC) by inhibiting multiple steps of androgen receptor (AR) signaling [21]. Yet, acquired resistance is still an unresolved problem, with reported limited Enzalutamide efficiency in PCa bone metastases [22], prompting studies to further search for novel contributors to the adaptive response in this microenvironment [23]. For instance, Kong et al. highlighted the likely crucial role in cholesterol-centered pathways in resistance to antiandrogen therapy [24].

Central issues in studying the contextual adipocyte-cancer cell crosstalk and effects of therapies are the use of 2D cell cultures, which present incomplete phenotypes, and the use of murine cells (murine adipocytes bearing significant differences to human adipocytes), both issues potentially misleading the discovery of new contributors to disease [25]. In the last ten years, *in vitro* 3D human models have enabled more accurate human adipocyte phenotypes, using extracellular matrix (ECM)-mimicking hydrogels such as fibrin [26], thiol-modified hyaluronic acid-based bioinks [27] and silk-alginate/silk [28,29], although mostly focused on recapitulating WAT. Despite acknowledged differences between WAs and BMAs, human 3D BMA models *in vitro* have been scarce, employing silk [30], porous polyester microspheres co-polymerized with gelatin, alginate, dextran, and pectin [31] and gelatin methacrylate (GelMA) hydrogels [32,33]. Fewer models were used in the context of adipocyte-cancer investigations, mostly in prostate cancer [32,34] and multiple myeloma [19,35,36] using human BMAs differentiated from mesenchymal stem cells, while most breast cancer studies used human WA-models [19,35,37,38]. GelMA hydrogels are particularly suitable and versatile as 3D cell culture platforms [39], due to a semisynthetic nature preserving some natural cues (e.g., RGD motifs) yet enabling mechanical tailorability to degrees of stiffness relevant to BMAT (<3 kPa elastic modulus) [40]. GelMA has demonstrated to relevantly maintain adipocyte phenotypes *in vitro* [32,33,41], being used to study adipokine expression levels under mechanical loads [33] and showing BMA delipidation when cocultured with prostate cancer cells [32]. While promising, those models are yet to be used to investigate biological questions more in depth, including assessing responses to therapies.

In this study, we introduce hyaluronic acid methacrylate (HAMA) hydrogels as a complementation of GelMA hydrogels and investigate their capacity to provide superior 3D adipogenesis of white- and bone marrow-derived progenitors (Simpson-Golabi-Behmel syndrome (SGBS) preadipocytes and bone marrow-derived mesenchymal stem cells). Hyaluronic acid-based hydrogels have shown particular promise for the engineering of adipose tissue for therapeutic purposes [42]. HAMA was previously utilized with GelMA in an acellular adipose tissue model, showing an enhancement in metabolic activities *in vivo* [43]. However, the study did not include groups with only GelMA or HAMA, thus failing to isolate and demonstrate the specific benefits of HAMA. Here we show that GelMA alone remains superior to HAMA or any HAMA/GelMA combinations as human adipose 3D models. Thus, we followed up and used only GelMA 4 % with no HAMA to derive our adipose tissue models for the rest of the study. We used them to test our hypothesis that the response of human metastatic prostate cancer cells to Enzalutamide would be reduced in the presence of human adipocytes, demonstrating microenvironment contribution towards resistance in an advanced PCa context. Using an indirect coculture of two types of human adipocytes (white-derived and bone marrow-derived) grown in GelMA, with metastatic human cancer lines (LNCaP, C4-2B) also grown in GelMA [32], we studied gene and protein dysregulation in the context of Enzalutamide treatment, in an all-human, all-3D, model of adipocyte-prostate cancer cell interactions.

2. Materials and methods

2.1. Cell culture

Two different types of adipocyte progenitor cells were used in the study. Human bone marrow mesenchymal stem cells (BM-MSCs, PCS500012, ATCC, USA) were used in passages 3–4. SGBS (human preadipocytes) cells were obtained from Dr Johanna Barclay (Mater Research, Qld, Australia) and used in passages 12–17. Prior to adipogenic differentiation, cells were cultured in adipocyte proliferation medium (APM, Table 1, all components from Thermo Fisher Scientific or Sigma-Aldrich, Australia. Rosiglitazone was purchased from Sapphire Bioscience, Australia).

Human prostate cancer cell lines, LNCaP and C4-2B (ATCC, USA), were used in passage 30–41 and cultured in cancer proliferation medium (CPM, Table 1). The use of human cells was covered by ethics approval

Table 1

Cell culture compositions. All percentages are vol/vol (v/v).

Media	Contents
Adipocyte Proliferation medium (APM)	DMEM, 10 % FBS, 1 %, penicillin/streptomycin (P/S), glutamine (200 mM), heparin (90 μg/mL), FGF-1 (1 ng/mL)
Adipogenic induction medium (AIM)	DMEM, 10 % FBS, 1 % P/S, glutamine (200 mM), heparin (90 μg/mL), FGF-1 (1 ng/mL), 3-Isobutyl-1-methylxanthine (IBMX, 500 μM), rosiglitazone (2 μM), dexamethasone (250 nM), insulin (10μg/mL), indomethacin (100 μM)
Adipogenic medium (AM)	DMEM, 10 % FBS, 1 % P/S, glutamine (200 mM), heparin (90 μg/mL), FGF-1 (1 ng/mL), IBMX (500 μM), dexamethasone (250 nM), insulin (10 μg/mL), indomethacin (100 μM)
Cancer proliferation medium (CPM)	RPMI 1640, 5 % FBS
Coculture medium (CoM)	DMEM, 10 % FBS, 1 % P/S, glutamine (200 mM)

(LR 2023-5612-12871) from QUT.

2.2. Cell encapsulation in photocrosslinkable GelMA and HAMA hydrogels

GelMA (porcine type A, 300 bloom, 80 % degree of functionalization) was purchased from Gelomics, Australia. HAMA was prepared according to Ref. [44]. Briefly, Hyaluronic Acid (HA, donated by Novozymes, Denmark) was dissolved in phosphate-buffered saline (PBS, Thermo Fisher) at 1 % w/v. HA was reacted with methacrylic anhydride (MAAh, Sigma-Aldrich, Australia; 5-fold molar excess MAAh over hydroxyl group) for 24h on ice, with the pH maintained at 8 using sodium hydroxide. After the reaction period, insoluble MAAh was removed by centrifugation, followed by dialysis in deionized water to remove remaining unreacted MAAh and methacrylic acid. The pH of the dialyzed polymer solutions was adjusted to 7.4, after which they were freeze-dried and stored at -20 °C until use. Prior to cell encapsulation, HAMA 3 % and GelMA 10 % w/v stock solutions were prepared in PBS and warmed up at 37 °C. Final precursor solutions were prepared by diluting the stock solutions in PBS, to 1 % or 2 % w/v for HAMA, and 1 % or 4 % w/v for GelMA. Four types of hydrogels were investigated in the study (HAMA 1 %, HAMA 2 %, HAMA 1%-GelMA 1 % and GelMA 4 %, all w/v). Prior to crosslinking, the precursor solutions were supplemented with 0.05 % w/v Irgacure 2959 (1-[4-(2-hydroxyethoxy)-phenyl]-2-hydroxy-2-methyl-1-propanone, BASF, Germany). Cell concentrations for SGBS cells and BM-MSCs were 2×10^6 cells/mL, for LNCaP 0.5×10^6 LNCaP cells/mL and 0.35×10^6 C4-2B cells/mL. PTFE moulds were used for hydrogel casting (5 mm × 2 mm), and hydrogels were crosslinked for 15 min at 365 nm (2.6 mW cm^{-2}, CL-1000 L, UVP, USA). After crosslinking and PBS rinsing, adipose hydrogels were placed in 48 well-plates (1 mL medium/well) and cultured in adipogenic proliferation medium (Table 1, APM) for 24 h, followed by adipogenic induction medium (1 mL medium/well, Table 1, AIM) for two days, followed by adipogenic medium (1 mL medium/well, Table 1, AM). Prostate cancer hydrogels were cultured in cancer proliferation medium (1 mL medium/well, Table 1, CPM). Acellular hydrogels were used for mechanical analysis (see below).

2.3. Coculture and treatments

Two days prior to coculture, adipose and prostate cancer hydrogels were cultured in 50 % of their corresponding media (AM for adipose, CPM for prostate cancer) and 50 % of coculture media (CoM, Table 1), before being placed within the same well in 48 well-plates for 1 week in 1 mL of CoM with DMSO (Sigma-Aldrich) as control, or Enzalutamide 10 μM (Selleck Chemicals), dissolved in DMSO. One media change was performed on day 4 (fully replenished), except for metabolic activity analysis with Prestoblue reagent (see below, done at day 1, 3, and 7).

2.4. Mechanical characterization

Acellular hydrogels were transferred to PBS immediately after crosslinking and allowed to reach swelling equilibrium overnight at room temperature before mechanical testing. Compressive mechanical testing (unconfined) was performed using an Instron 5848 Microtester, 5 N load cell (Instron) in a PBS bath maintained at 37 °C. HAMA, HAMA/GelMA, and GelMA hydrogels (n = 6) were immersed in the PBS bath and compressed at a displacement rate of 0.01 mm/s. Prior to testing, the surface area of each gel was determined using a stereomicroscope and ImageJ software. Young's moduli were calculated as the slope of the stress/strain curves (between 10 and 15 % strain) according to Ref. [45].

2.5. Viability and metabolic activity

Cell viability in the adipose hydrogels at day 1 was assessed using fluorescein diacetate/propidium iodide staining (FDA/PI, Sigma-Aldrich). Hydrogels were washed with PBS and incubated with FDA (1 μg/mL) and PI (5 μg/mL) in PBS for 10 min at 37 °C. Upon PBS rinsing (twice, 5 min, 37 °C), they were immediately imaged with green (ex: 488 nm) and red (ex: 561 nm) filters, using a Spectral Spinning Disc Confocal (SDC) Microscope (Nikon, Japan) using 250 μm thick z-stacks and a step size of 10 μm. The metabolic activity of adipose and prostate cancer hydrogels alone, or individually after coculture, was assessed using the Prestoblue reagent (Thermo Fisher) at day 1 (prior to coculture), 3 and 7. A volume of 1 mL/well (90 % medium, 10 % reagent) was added to the well and incubated for 3 h and 30 min at 37 °C. The supernatants were transferred in triplicates (100 μL) in 96 well-plates and fluorescence was read using CLARIOstar (BMG Labtech, Germany) at ex: 560 nm, em: 590 nm. Hydrogels were washed twice with PBS (5 min, 37 °C) and replaced with their corresponding media and incubated until the next datapoint. Data was subtracted from acellular hydrogels.

2.6. Immunofluorescence and lipid staining

Cell and spheroid morphology: The 3D morphologies of PCa spheroids and adipocytes were assessed by immunostaining and confocal imaging. At desired times, hydrogels were washed twice in PBS and fixed in 4 % paraformaldehyde (PFA, Thermo Fisher) for 30 min at room temperature, permeabilized using Triton 0.2 % v/v (Sigma-Aldrich) for 20 min and incubated in 5 % w/v bovine serum albumin (BSA, Sigma-Aldrich) for 2 h. Constructs were then stained with 4′,6-diamidino-2-phenylindole (DAPI, Sigma-Aldrich, 5 μg/mL) and fluorescein isothiocyanate–conjugated Phalloidin (200 U/mL, Alexa Fluor™ Phalloidin-488, A12379, Thermo Fisher) and incubated overnight on a rocker at 4 °C (150 μL/well). After two washes (in PBS, on rocker, 15 min each) at room temperature, the third PBS wash was done overnight on a rocker at 4 °C. Images were taken using the SDC microscope (Nikon), using blue (ex 405 nm) and green (ex 488 nm) filter sets for nuclei and F-actin filament visualization, respectively. Maximal intensity projections were made from z-stacks (250 μm thickness, 10 μm step size for 4 × and 10 × magnifications, 100 μm thickness, 5 μm step size for 20 × magnification). Image-based quantification of spheroid sizes from 10 × magnification images were conducted using QuPath software (version 0.4.4) and modified StarDist algorithm.

Adipokine receptor visualization: For visualization of leptin receptor (LEPR, ab60042 Abcam, USA) and adiponectin receptor 1 (ADIPOR1, ab126611, Abcam), hydrogels were immersed overnight in 1 % w/v BSA primary antibody solutions (1:400 dilutions) on a rocker at 4 °C (150 μL/well). After two washes (in PBS, on rocker, 15 min each) at room temperature, the third PBS wash was done overnight at 4 °C. The next day, PBS was removed and replaced with 1 % w/v BSA secondary solutions (DAPI 5 μg/mL, Phalloidin-488 1:200 and goat anti-Rabbit IgG Alexa Fluor 555 1:200, ab150086, Abcam) and incubated overnight on a rocker at 4 °C (150 μL/well). After two washes (in PBS, on rocker, 15 min each) at room temperature, the third PBS wash was done overnight

on a rocker at 4 °C. Images were taken with the SDC microscope using blue (ex 405 nm), green (ex 488 nm), and red (ex 650 nm) filter sets. Maximal intensity projections were made from z-stacks (130 μm thickness, 2.5 μm step size, 10 × magnification images).

Lipid droplet visualization: Two methods were used to assess lipid droplets, using Oil Red O (ORO, Sigma-Aldrich) for phase contrast imaging and nile red (Sigma) for fluorescence imaging, after PFA fixation (7 min for 2D cells and 30 min for hydrogels at room temperature). For ORO, cells and hydrogels were immersed 15 min in isopropanol 60 % v/v (Thermo Fisher), then stained for 1 h with a freshly prepared 3 mg/mL ORO solution. Upon rinsing with distilled water, 2D cells and hydrogels were imaged using phase contrast microscopy. For nile red, adipose hydrogels were incubated overnight with a solution of 10 μg/mL of nile red at 4 °C in the presence of DAPI/Phalloidin (as explained previously). Images were taken with a SDC microscope using red (ex 650 nm) filter sets. Maximal intensity projections were made from 250 μm thick z-stacks, 10 μm step size, 10 × magnification images. Image-based quantification of lipid droplets positive cells was performed using ImageJ analysis software (version 1.54f, National Institute of Health (NIH), USA).

2.7. Enzyme-linked immunosorbent assay (ELISA)

The levels of leptin and adiponectin high molecular weight (HMW) in the conditioned cell culture media were determined using ELISA kits (R&D Systems, USA) on adipose hydrogels alone after 3 weeks of differentiation or in coculture with prostate cancer hydrogels ($N = 3$ biological replicates, $n = 2$–3 technical replicates). Briefly, conditioned media were collected at day 1, 3, 7 and stored at −20 °C until analysis. The samples were brought to room temperature before analysis using the kits as per the manufacturer's protocols using standard curves and a microplate reader (FLUOstar Omega, BMG Labtech, Germany), set to 450 nm with wavelength correction at 540 nm.

2.8. Seahorse assay

The metabolism of 2D adipocytes ± Enzalutamide 10 μM was studied using the seahorse XFe96 extracellular flux analyzer (Agilent Technologies Inc., USA) according to Ref. [46]. SGBS-derived adipocytes were cultured in a 2D seahorse XFe96 well-plate (reversed shape with a flat bottom). After 14 days of adipogenic differentiation, a mitochondrial stress test (MST) assay, a glycolysis assay and a fatty acid oxidation (FAO) assay were performed. The day before the assay, the probe plates were hydrated with Nano Pure water (LifeSciences, Australia, 200 μL/well). On the day of the assay, water was discarded and 200 μL of the pre-warmed XF calibrant (Agilent) was added to each well. The sensors were submerged and placed back in a non-CO₂, 37 °C incubator for 45 min. The media for the MST and the glycolysis assay were prepared by adding the necessary supplements to the base media, for the FAO assay to sterile Nano Pure water (Supp. Table 1) and warmed to 37 °C. The pH was adjusted to 7.4 ± 0.1. The media was filter-sterilized (0.2 μm) and the cells were washed with the respective assay medium. All but 20 μL of media were removed from each well, then 200 μL of the respective assay media were added. After media removal, the wells for MST and glycolysis assay received 160 μL of the respective media to a total volume of 180 μL in each well. For the FAO assay, 100 μL of FAO assay media were added to a total volume of 120 μL. The plate was placed in a non-CO₂, 37 °C incubator for 1 h to archive atmospheric oxygen concentration in the media. The required injection compounds were prepared (Supp. Table 1) and loaded in the sensor cartridge. The compounds were gently dispensed in the respective ports. For a 10 × dilution in the assay media, 20 μL of Injection A, 22 μL of Injection B and 25 μL of Injection C were added to Port A, B and C respectively (Supp. Table 1). Next, the setup was analyzed using the Wave Analyzer software and the following protocol was set up: measure 2 ×, inject Port A, measure 3 ×, inject Port B, measure 3 ×, inject Port C, measure 3 ×.

After assay completion, the media was removed from all wells, the plate was frozen at −80 °C for DNA content assessment using a Quant-iT PicoGreen dsDNA Assay Kit (Invitrogen).

A volume of 180 μL of 0.5 mg/mL proteinase K (Invitrogen) diluted in filtered (0.2 μm) phosphate buffered EDTA (PBE, disodium phosphate, monosodium phosphate and disodium ethylenediaminetetraacetate dehydrate in deionized water) was added to each well for overnight incubation (37 °C). The samples were incubated at 56 °C for 8 h prior to analysis. A standard dilution series using a λ DNA standard from the Quant-iT PicoGreen dsDNA Assay Kit (Invitrogen) in PBE was pipetted in each of three black 96 well plates in triplicates. The Seahorse samples were then diluted 1:1.5 and pipetted in duplicates. The PicoGreen staining solution was prepared by diluting the supplied dye 1:200 in 1 × Tris EDTA (TE) buffer. To each standard or sample, 100 μL of PicoGreen dye solution was added and incubated for 10 min. The plate was analyzed by measuring the fluorescence (ex: 485 nm, em: 520 nm) using the FLUOstar Omega spectrophotometer, the corresponding Omega 5.11 software and the 3.20 R2 MARS Data Analysis Software by BMG Labtech. The results were analyzed using a 4-parameter fit. The measured oxygen consumption respiration (OCR) in pmol/min and extracellular acidification rate (ECAR) in mpH/min was analyzed using the Wave Desktop 2.6 software (Agilent) and normalized to the measured DNA content/well in ng/ml with a scale factor of 100. For the FAO test the difference between the wells treated with Etomoxir (Eto) and non-Eto treated wells was analyzed.

2.9. Gene expression

Hydrogels were washed twice for 5 min in PBS, and two hydrogels per condition were pooled together in 1 mL of TRIZol reagent (Invitrogen) for 20 min before −80 °C storage for at least 48 h until RNA extraction. Upon thawing to room temperature, hydrogels were mechanically broken into small pieces by repeatedly passing through 21G needles, and centrifuged at 16,000 rpm for 1 min to remove cell and hydrogel debris. mRNA was extracted from TRIZol reagent using Directzol RNA Miniprep Plus Kit (Zymo Research, USA) following the manufacturer's protocol. mRNA (250 ng) was reverse transcribed into cDNA (SensiFast cDNA Synthesis Kit, Bioline, Australia). Quantitative PCR was performed using SYBR Green PCR Master Mix (Thermo Fisher) and QuantStudio 6 Flex System (Applied Biosystems, USA). *7SL*, *RPL32* and *Cyclophilin* were used as housekeeping genes to normalize the Cq values for each marker (Table 2), and differential gene expression was calculated using the ΔΔCq method.

2.10. Statistical analysis

Plots were generated using GraphPad Prism version 10.1.2. In legends, SD refers to standard deviation and SE refers to standard error. All statistical analyses were performed in IBM SPPS Statistics version 29.0.0.0 (IBM Corp.) using a univariate general linear model and assessing parameter estimates using a posthoc Tukey test, when overall significance was achieved. Significance level was determined as *$p < 0.05$, **$p < 0.01$, ***$p < 0.001$, and ****$p < 0.0001$.

3. Results

3.1. Softer GelMA hydrogels provide enhanced adipogenesis compared to stiffer HAMA and GelMA/HAMA hydrogels

GelMA hydrogels (4 % w/v) were previously shown to support adipogenic differentiation of human preadipocyte cells derived from white adipose tissue (SGBS cells) and mesenchymal stem cells extracted from the bone marrow (BM-MSCs) up to 28 days [32]. As no significant differences were observed in lipid droplet size and adipogenesis genes between cell types, GelMA 4 % was proven to be a versatile and robust model to obtain mature human adipocytes *in vitro*, to be used according

Table 2

Primers sequences used for RT-qPCR.

Target Gene	Primers (5′-3′)
PPARγ	F: GAAACTTCAAGAGTACCAAAGTG, R: AGGGCTTATTGTAGAGCTGAGTCTTCTC
FABP4	F: GGATGATAAACTGGTGGTGGAATG, R: CAGAATGTTGTAGAGTTCAATGCGA
C\EBPα	F: CCAAGAAGTCGGTGGACAAGAAC, R: CACCTTCTGCTGCGTCTCCA
PLIN1	F: ACCCCCCTGAAAAGATTGCTT, R: GATGGGAACGCTGATGCTGTT
GLUT4	F: ATGCTGCTGCCTCCTATGAA, R: CAGTTGGTTGAGCGTCCC
FASN	F: CGCTCGGCATGGCTATCT, R: CTCGTTGAAGAACGCATCCA
ADIPOQ	F: AGTCTCACATCTGGTTGGGG, R: CTCTCTGTGCCTCTGGTTCC
LEP	F: CGGATTCTTGTGGCTTTGG, R: TGACTGCGTGTGTGAAATG
CD36	F: CTTTGGCTTAATGAGACTGGGAC, R: GCAACAAACATCACCACACCA
ACYL	F: GACTTCGGCAGAGGTAGAGC, R: TCAGGAGTGACCCGAGCATA
ATGL	F: GTGTCAGACGGCGAGAATG, R: TGGAGGGAGGGAGGGGATG
ACACA	F: TCGCTTTGGGGAAATAAAGTG, R: ACCACCTACGGATAGACCG
LIPE	F: GCGGATCACACAGAACCTGGAC, R: AGCAGGCGGCTTACCCTCAC
PSA	F: AGTGCGAGAAGCATTCCCAAC, R: CCAGCAAGATCACGCTTTTGTT
AR	F: CTGGACACGACAACAACCAG, R: CAGATCAGGGGCGAAGTAGA
DPPIV	F: CAAATTGAAGCAGCCAGACA, R: CACACTTGAACACGCCACTT
ARV7	F: AGCCGCTGAAGGGAAACAGAAG, R: TTTGAATGAGGCAAGTCAGCCTTTCT
7SL	F: ATCGGGTGTCCGCACTAAGTT, R: CAGCACGGGAGTTTTGACCT
RPL32	F: GCACCAGTCAGACCGATATG, R: ACTGGGCAGC ATG GCTTTG
Cyclophilin	F: CGCGTCTCCTTTGAGCTGTT, R: TCTCCAGTGCTCAGAGCACG

to contextual adipocyte study needs (WAT or BMAT) [32]. As hyaluronic acid is a contributing component of the bone tumor microenvironment [47], and was previously shown to positively support adipose tissue engineering using porcine adipose-derived stem cells *in vitro* [48], and *in vivo* [42], we investigated if there were any benefits in complementing GelMA with a hyaluronic acid methacrylate (HAMA) hydrogel or using HAMA hydrogels alone (Fig. 1A). The results (Fig. 1B–D) showed that even at minimal concentrations (HAMA 1 % w/v), the stiffness values of HAMA acellular gels were higher than GelMA 4 % (Fig. 1B, $p < 0.0001$), and that the addition of GelMA 1 % to HAMA 1 % did not significantly change stiffness values compared to HAMA 1 % alone ($p = 0.16$). Unlike prior mechanical studies of HAMA [49], doubling the concentration from HAMA 1–2 % w/v resulted in a 1.5-fold increase in stiffness (5.4 $\pm$ 0.5 to 8.2 $\pm$ 1.0 kPa, $p < 0.0001$).

Upon encapsulation of the two cell types, >98 % viability was observed in all four hydrogel types at day 1 (Fig. 2A). After 21 days of culture, morphological observations and staining of lipid droplets confirmed >90 % of cells were positive with lipid droplets (Fig. 2B). As previously demonstrated in most studies of adipocytes grown *in vitro* (2D and 3D), all differentiated cells in all four hydrogel types presented multiple smaller lipid droplets per cell (Fig. 1D), as opposed to one single large droplet per cell as seen *in vivo* [50]. While there was no difference in adipocyte size between cell types (Fig. 2C middle, $p = 0.3$), an increase in total lipid content (ORO + area) was seen in SGBS-derived adipocytes, overall (Fig. 2C bottom, $p < 0.0001$). Hydrogel type however led to dramatic differences on both cell size and lipid content (Fig. 2C, $p < 0.0001$). Decreased stiffness was directly correlated with increased adipocyte size and lipid content. As for same stiffness but
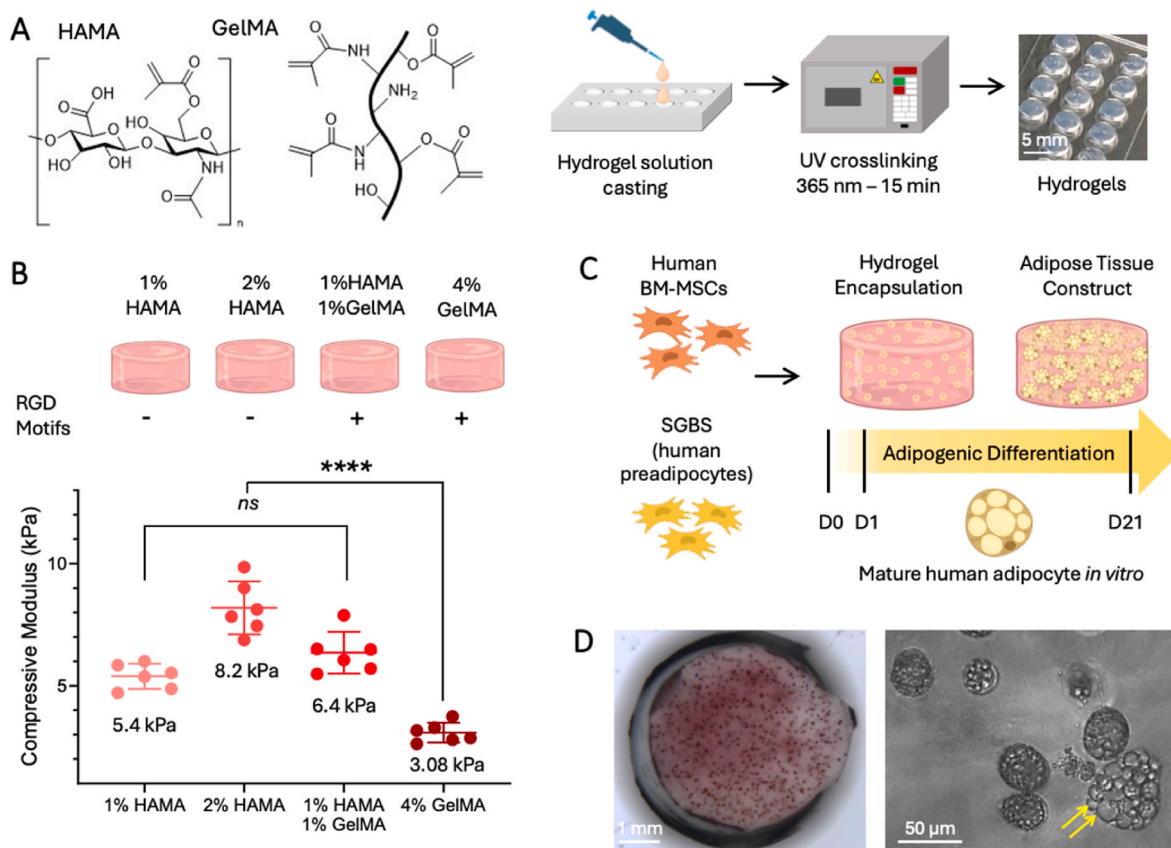
Fig. 1. Experimental design and mechanical properties. A) Hyaluronic Acid Methacrylate (HAMA) and Gelatin Methacryloyl (GelMA) molecules, schematic of the hydrogel manufacturing process and resulting crosslinked hydrogels. **B)** Schematic of the four types of hydrogels investigated in this study and their compressive moduli (acellular, $n = 6$, means $\pm$ standard deviation (SD), univariate general linear model, *ns*: non-significant, **** = $p < 0.0001$). **C)** Hydrogel encapsulation of human primary cells (BM-MSCs: bone-marrow mesenchymal cells, SGBS: Simpson-Golabi-Behmel syndrome preadipocytes) and adipogenic differentiation for 21 days. **D)** Representative stereomicroscopy (left) and bright field images (right) of Oil-Red-O-stained mature adipocyte-laden GelMA hydrogels (4 % w/v, arrows show lipid droplets) after 21 days of differentiation.
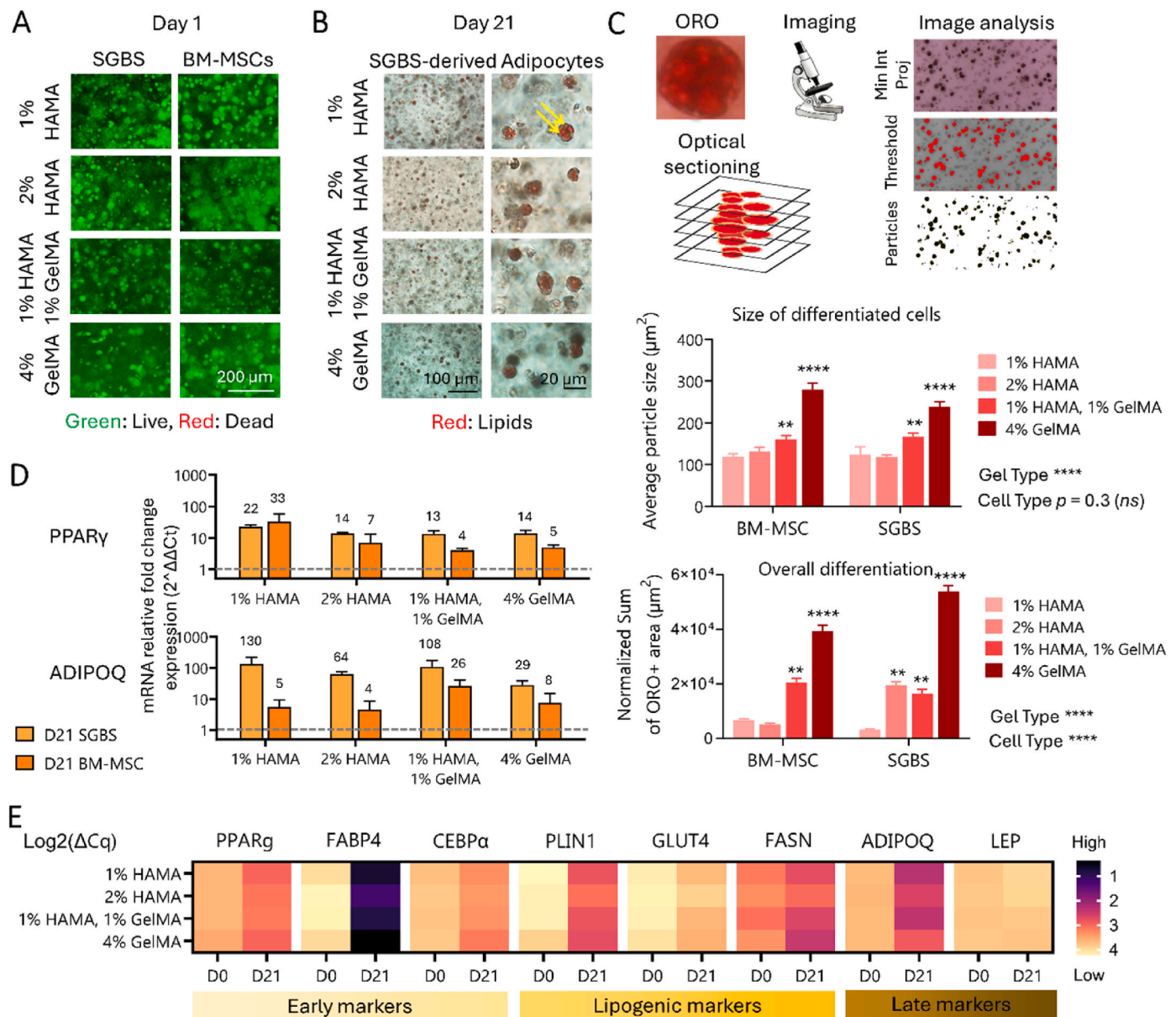
Fig. 2. Adipogenesis in methacryloyl hydrogels. A) Confocal microscopy images (maximal projections, 250 μm z-stacks) of cells (BM-MSCs: bone-marrow mesenchymal cells, SGBS: Simpson-Golabi-Behmel syndrome preadipocytes) encapsulated in different hydrogel types (HAMA: hyaluronic acid methacrylate, GelMA: gelatin methacryloyl) at day 1 post encapsulation and FDA/PI staining for viability (green = live, red = dead). **B)** Brightfield images of Oil-Red-O (ORO) lipid-stained mature adipocytes after three weeks of differentiation. **C)** Schematic of the processing pipeline for quantitative assessment of ORO staining and resulting particle size and overall differentiation across gels (Average $n = 136$ cells, top; $n = 3$ fields of view, bottom; means ± standard error (SE), univariate general linear model, significance shown against 1 % HAMA: ** = $p < 0.01$, *** = $p < 0.001$, **** = $p < 0.0001$). **D)** mRNA relative expression levels after 21 days of adipogenic differentiation, normalized to D1 SGBS or BM-MSC (where relevant), within each hydrogel type. **E)** mRNA mean Log2(ΔCq) heatmap of differentiated adipocytes from SGBS. Black represents higher mRNA expression (i.e., lower Log2(ΔCq)) and pale yellow represents lower mRNA expression (i.e., higher Log2(ΔCq)). For panels D and E, $N = 3$ biological and $n = 3$ technical. Results were normalized to the geomean of *7SL* and *RPL32* as housekeeping genes.

different gel compositions (i.e., 1 % HAMA versus 1 % HAMA,1 % GelMA), the presence of GelMA significantly increased adipocyte size and lipid content for adipocytes derived from both cell types (Fig. 2C, $p < 0.01$), demonstrating the added benefits of GelMA for adipose tissue models, likely due to the presence of RGD motifs that were absent in HAMA [51]. Across all gels and cell types, lower stiffness GelMA 4 % was deemed superior for adipogenesis compared to higher stiffness HAMA and HAMA/GelMA combinations in both differentiated cell types and lipid content. Gene expression did not show significant differences between hydrogel groups (Fig. 2D), with the main differences being between cell types, such as lower *PPARγ* (early adipogenic marker) and *ADIPOQ* (late marker) for adipocytes derived from BM-MSCs, in line

with previous results in adipocytes differentiated for 14 or 28 days [32], versus 21 days here. Adipogenesis was successful in all four hydrogels with no major differences across hydrogels (Fig. 2E) and increased expression of early adipogenesis genes (*PPARγ*, *FABP4*, *CEBPα*), lipogenic markers (*PLIN1*, *GLUT4*, *FASN*) and late markers, important in cancer (e.g., *ADIPOQ* [25]), obtained from encapsulation of undifferentiated cells to mature adipocytes in 3 weeks of *in vitro* adipogenic differentiation culture.

Overall, it can be concluded that both cell types provided similar degrees of adipogenesis in all 3D hydrogels of this study, with only a slightly higher differentiation trend for SGBS-derived hydrogels (both at gene and lipid content levels), as can be expected due to their

precommitted lineage to adipocytes [52]. Without major differences compared to other hydrogels at gene level, but a significantly superior advantage in terms of increased lipid content and adipocyte size, the use of softer GelMA 4 % hydrogels was selected for subsequent studies.

3.2. Human adipocytes and prostate cancer cells in 3D hydrogel coculture led to increased leptin and decreased adiponectin levels

After validating GelMA 4 % as an adipose model containing mature human adipocytes, we cocultured the bioengineered adipose tissues with PCa microtissues comprising of metastatic androgen receptor (AR) PCa cell lines, LNCaP cells (AR+, androgen-dependent) or a more aggressive line; C4-2B cells (AR+, androgen-independent) in GelMA 4 % too, as previously established [32], cultured separately to first establish PCa spheroids larger than 50 μm, and depicted in Fig. 3A. Using optimized 3D protocols [33], we applied immunofluorescence, brightfield and confocal microscopy (Fig. 3B), to look at morphological and protein changes in both cancer spheroids and adipocytes, as cultured together, yet in separate hydrogels.

First, adipose and cancer hydrogels were cocultured for 7 days without Enzalutamide (Fig. 4A) with the hypothesis that paracrine interactions may cause dysregulations at the gene level but may not be sufficient to cause delipidation of adipocytes, as this explicit phenomenon has always been observed in adipocytes in close proximity to the cancer in the *in vivo* microenvironment only [53–55]. Metabolic activity (Prestoblue assay) increased over the 7 days of culture only for all SGBS-derived adipose hydrogel groups (Fig. 4Bi, $p < 0.001$) and was significantly different in coculture with cancer cells only for those gels (Fig. 4Bi-I, $p < 0.0001$). In coculture, metabolic activity dropped after as early as 1 day of culture only for SGBS-derived adipose hydrogels. None of these changes were reported for BM-MSC-derived adipose hydrogels (Fig. 4Bii, $p > 0.05$). Similar to a previous study done with the same cell types [32], yet cultured in *direct* contact inside the same hydrogel, here the LNCaP and C4-2B cancer spheroids did not display metabolic

activity differences upon *indirect* coculture with the adipose hydrogels (Fig. 4Biii-iv, $p > 0.05$). While initial qualitative morphological analysis suggested an increase in spheroid size for both LNCaP and C4-2B (Fig. 4C left), no obvious changes in adipocyte delipidation or size reduction could be recorded (Fig. 4C right), although fibroblast-like morphology was sporadically observed. From a gene expression point of view, adipocytes tended to be more dysregulated upon coculture with LNCaP spheroids than C4-2B spheroids (Fig. 4D left). While leptin (*LEP*), known to induce proinflammatory signaling that serves cancer survival [56], seemed to be increased after coculture with LNCaP spheroids, this was non-significant (Fig. 4D right). In cancer cells, no alterations were found within the study timeframe, to the exception of a non-significant FABP4 increase in LNCaP (although not seen in C4-2B, Fig. 4D right), in line with previous reports [7,57].

We studied the protein levels of leptin and adiponectin, two key adipokines implicated in cancer, within SGBS-derived adipose hydrogels. We further investigated how these levels were dysregulated when cocultured with LNCaP and C4-2B microtissues. First, their expression profiles showed increased leptin and decreased adiponectin by day 7 (Fig. 5A), compared to the baseline adipocytes alone (without PCa coculture). In PCa microtissues alone, there was minimal expression of both adipokines in the media (Fig. 5B, lighter green bars). Upon coculture with the adipose microtissues however, leptin expression in media was even higher than adipose hydrogels alone (Fig. 5B left), in line with the well-known protumoral effect of leptin [58]. PCa cells expressed the leptin receptor in smaller spheroids only (<40 μm, Fig. 5C), suggesting an early-stage use of leptin receptor expression in tumor formation, which may disappear once the spheroid reaches a certain size and becomes self-sustaining. Conversely, adiponectin receptor initially found in smaller size spheroids was reduced upon coculture with cancer cells (Fig. 5C) and reduced in media from SGBS alone (Fig. 5B), in line with the antitumoral effect of adiponectin inhibiting Akt, STAT3 and mTOR pathways [59].

Overall, these results highlight the suitability of GelMA hydrogels as
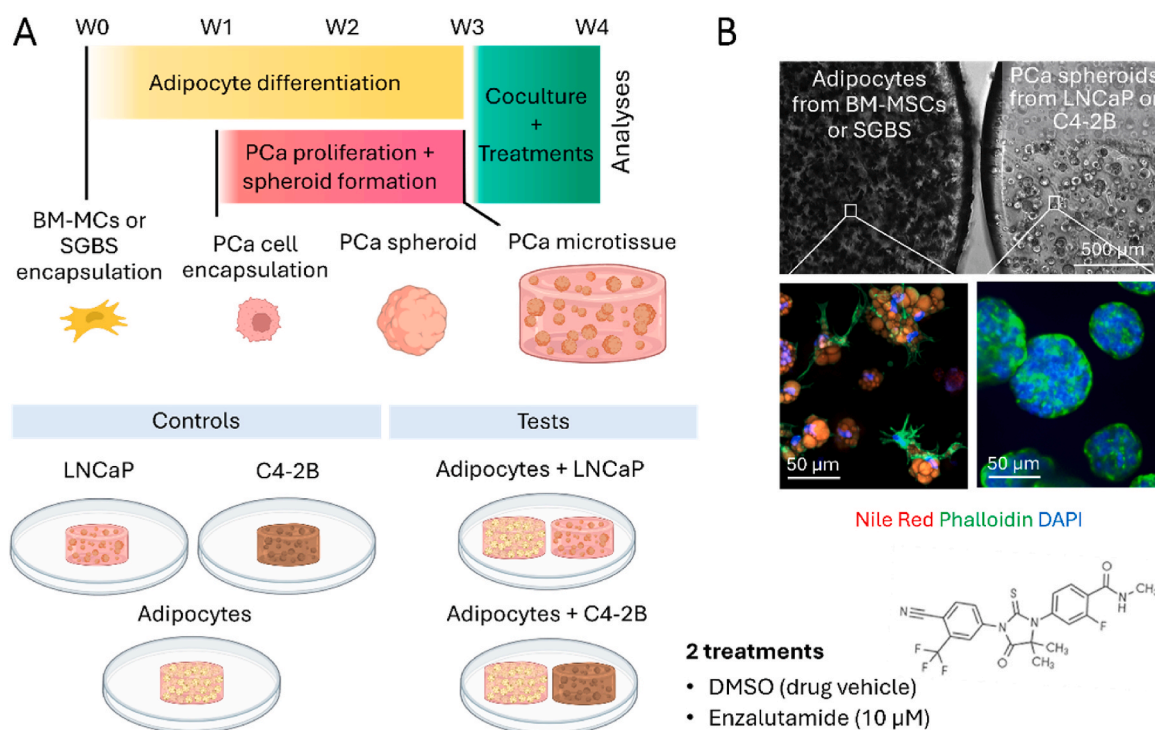
Fig. 3. Experimental design for indirect 3D cocultures between human adipocytes and human prostate cancer cells grown in GelMA hydrogels. A) Timeline and components. Hydrogels (4 % w/v GelMA) contain only one type of cell and are either cultured in monoculture or in coculture. **B)** Representative brightfield and confocal images following immunofluorescence staining (Blue/DAPI = cell nuclei, green/phalloidin = actin, red/nile red = lipid droplets) of GelMA hydrogels containing either PCa spheroids or mature adipocytes after one week of coculture and treatment.
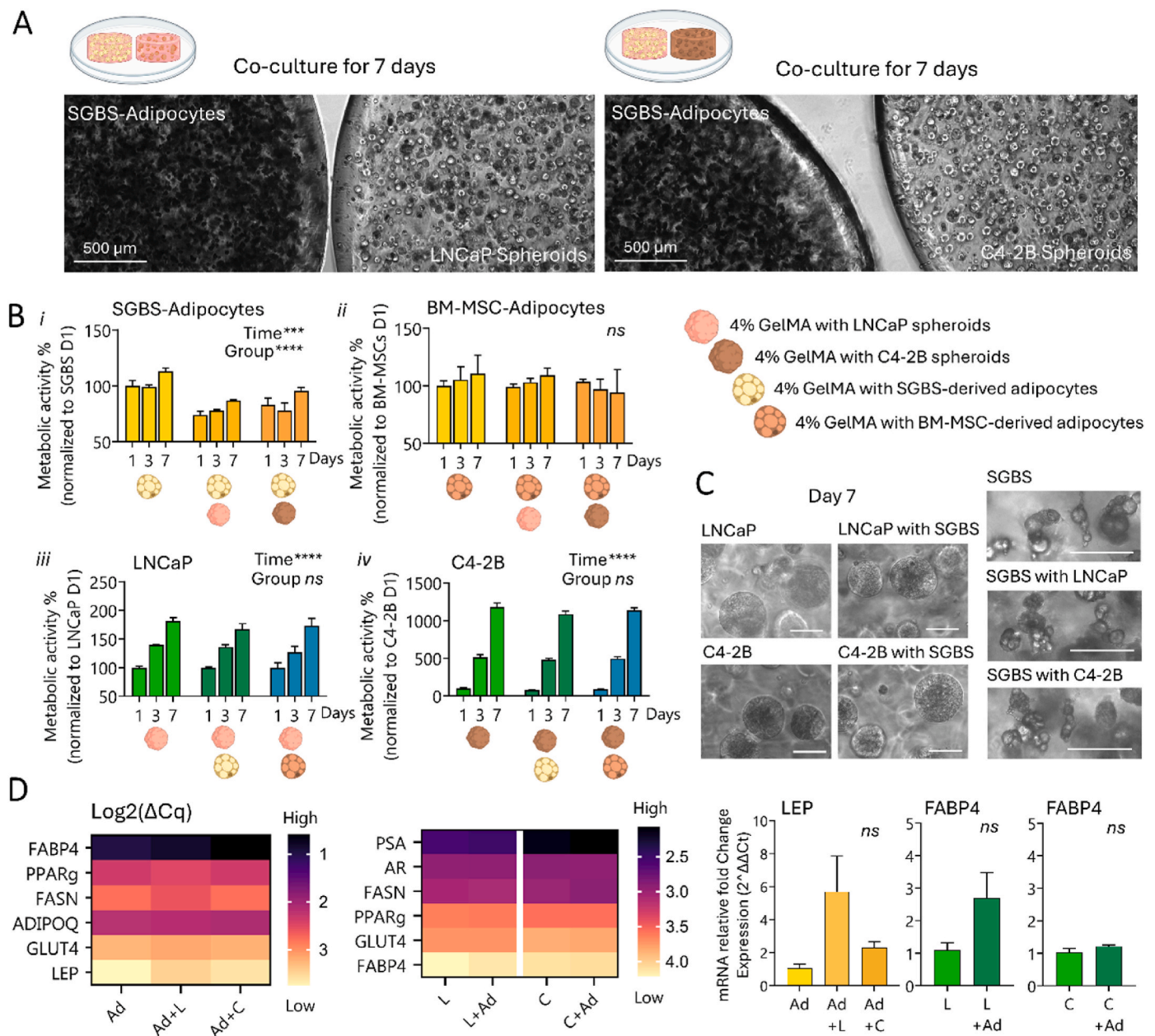
Fig. 4. Reciprocal paracrine effects of human adipocytes and human prostate cancer spheroids grown in GelMA hydrogels. A) Schematic of indirect cocultures and brightfield images after 7 days of coculture. **B)** Top: Metabolic activity over 7 days of (*i*) SGBS-derived adipocytes, (*ii*) BM-MSC-derived adipocytes in gelatin methacryloyl hydrogels (GelMA), cultured either alone or with an adjacent GelMA hydrogel containing either LNCaP spheroids or C4-2B spheroids. Bottom: Metabolic activity over 7 days of (*iii*) LNCaP spheroids, (*iv*) C4-2B spheroids in GelMA, cultured either alone with an adjacent GelMA hydrogel containing either SGBS-derived adipocytes or BM-MSC-derived adipocytes. Means ± standard error (SE) shown ($n = 4$–12), univariate general linear model: *** = $p < 0.001$, **** = $p < 0.0001$. **C)** Brightfield images of LNCaP and C4-2B spheroids and SGBS-derived adipocytes in their individual GelMA hydrogels after 7 days of mono- or coculture. Scale bar = 100 μm. **D)** mRNA levels shown by mean Log2(ΔCq) heatmap and mRNA relative fold changes (normalized to Ad, L and C) after 7 days of mono- or coculture. For heatmap, black represents higher mRNA expression (i.e., lower Log2(ΔCq) and pale yellow represents lower mRNA expression (i.e., higher Log2(ΔCq)). $N = 3$ biological and $n = 3$ technical, means ± SE shown for relative fold changes, and results were normalized to the geomean of *7SL* and *Cyclophilin* as housekeeping genes. Ad: SGBS-derived adipocyte hydrogel, L: LNCaP hydrogel, C: C4-2B hydrogel, Ad + L: SGBS-derived adipocyte hydrogel after coculture with LNCaP hydrogel, Ad + C: SGBS-derived adipocyte hydrogel after coculture with C4-2B hydrogel. *ns*: non-significant.

a versatile platform for adipogenesis of human progenitors, tumor spheroid formation for metastatic PCa cells, and mechanistic and adipokine analysis under coculture. With SGBS-derived adipocytes displaying an increased degree of sensitivity in coculture with cancer cells, they suggest that white adipocytes may lead to more paracrine dysregulation in the tumor context and represent an ideal model for non-bone metastases (i.e. from visceral, lymph node, liver, lung sites) for advanced PCa under antiandrogen therapy.

3.3. Enzalutamide treatment dysregulates adipocyte metabolism in 2D

The delipidation process in adipocytes in both primary and metastatic niches has been suggested to arise from the alterations generated by the presence of cancer cells in the local tumor microenvironment [30, 50]. Yet, little is known on the effects of cancer treatments on the adipocytes *per se,* and whether this could contribute to treatment resistance or favor metastatic progression in a 'primed' adipocyte-rich niche.
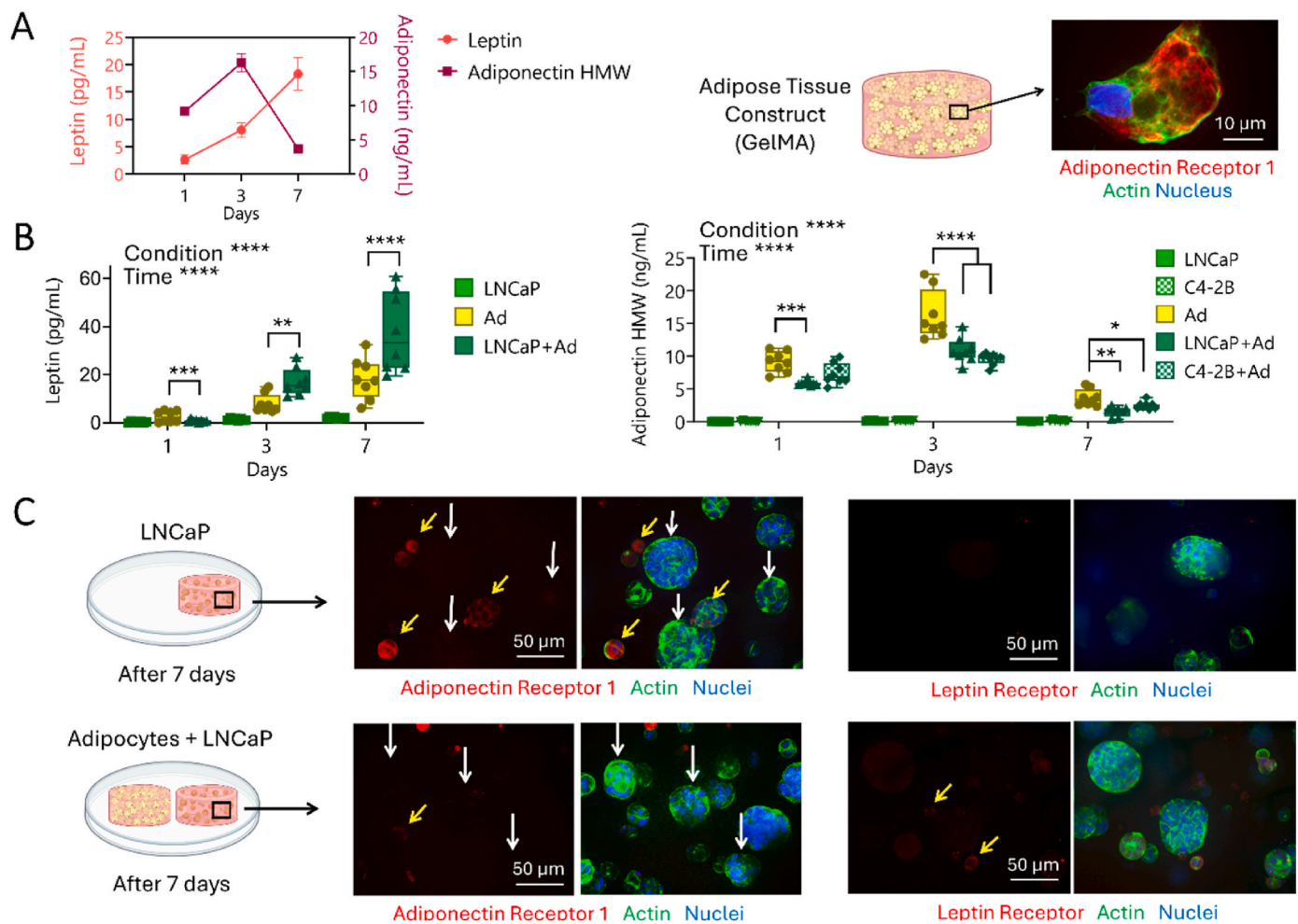
Fig. 5. Adipokines and their receptor dysregulateduponPCa cell-adipocytecoculture. **A)** Levels of Leptin and Adiponectin in adipocytes derived from SGBS in gelatin methacryloyl hydrogel (='adipose tissue construct') over 7 days, after prior differentiation for three weeks, as measured by ELISA ($N = 3$, total $n = 8$, means ± standard error (SE)), and corresponding confocal image of a 3D adipocyte in hydrogel stained for adiponectin receptor (Blue/DAPI = nuclei, green/phalloidin = actin, red = adiponectin receptor 1). **B)** Levels of leptin and adiponectin high molecular weight (HMW) for various hydrogel conditions (mono- and cocultures) as measured by ELISA ($N = 3$, total $n = 8–9$, box plots, univariate general linear model, * = $p < 0.01$, ** = $p < 0.001$, *** = $p < 0.001$, **** = $p < 0.0001$). **C)** Schematic and confocal images of LNCaP spheroids in 4 % GelMA in mono- and coculture with SGBS-derived adipose tissue construct (Blue/DAPI = nuclei, green/phalloidin = actin, red = adiponectin receptor 1 or leptin receptor). Yellow/tilted arrows show staining, white/vertical arrows show absence of staining.

Enzalutamide, the gold standard AR pathway inhibitor for CRPC, has been shown to powerfully inhibit AR signaling and activate a number of adaptive pathways associated with treatment resistance [23]. Considering the large incidence of adipocytes in metabolically deregulated CRPC metastatic microenvironments, we sought to investigate the research question sequentially. First, we used a simplified 2D culture model (2D adipocytes and Enzalutamide treatment) so that we could undertake metabolic analysis (Seahorse assay). Then we used the 3D culture cancer model established previously (3D adipocytes in GelMA ± coculture with PCa spheroids in GelMA under Enzalutamide treatment) for other analysis (Seahorse XF96 machine has unreliable sensitivity in 3D).

The 2D culture of adipocytes derived from SGBS and BM-MSCs and treated with Enzalutamide for either 7 or 14 days is presented in Fig. 6A. Looking at the controls, the gene expression profile was similar between cell types although the lipid transporter *CD36*, and *FABP4*, tended to be more expressed in SGBS-derived adipocytes (Fig. 6B). Under Enzalutamide, no significant differences were observed after 7 days of culture for any of the genes analyzed (all within 0.5–1.5-relative fold changes, considered non-significant), except for *LEP*, and in opposite trends. Indeed, Enzalutamide downregulated *LEP* in SGBS-adipocytes (0.41 ± 0.06 fold, $p < 0.01$), while it upregulated *LEP* in BM-MSC-adipocytes

(1.86 ± 0.06 fold, $p < 0.01$), critically showing how adipocytes from different tissues (subcutaneous and bone marrow) can respond differently to the same treatment. While no morphological differences were seen after 7 days at cellular levels, both types of adipocytes appeared to have lower lipid content suggesting reduction in lipid size (Fig. 6C) after 14 days of culture. Upon ORO staining (Fig. 6D) and analysis via two different methods (Fig. 6E–F), Enzalutamide did cause a decrease in ORO intensity (0.9-fold for SGBS-adipocytes, and 0.7 for BM-MSC-adipocytes), yet this was not significant for any of the cell types. We went further and performed, for the first time to our knowledge, a metabolic analysis on adipocytes subjected to Enzalutamide. The results strikingly showed that for all typical analyses of metabolic activity, including fatty acid oxidation (FAO), mitochondrial respiration and glycolytic function (Fig. 6G–H, Supp. Fig. 1), Enzalutamide significantly increased oxygen consumption respiration (OCR) for maximal FAO ($p < 0.05$) and extracellular acidification rate (ECAR) for maximal glycolysis ($p < 0.05$, Fig. 6H). Correlating with the trends of reduced lipid droplet sizes, this data suggests that Enzalutamide may prime adipocytes to releasing FFAs via endocrinal pathways. This may be a key contributor towards the attraction of circulating cancer cells to the adipocyte-rich bone microenvironment in a system not yet metastasized to the bone.
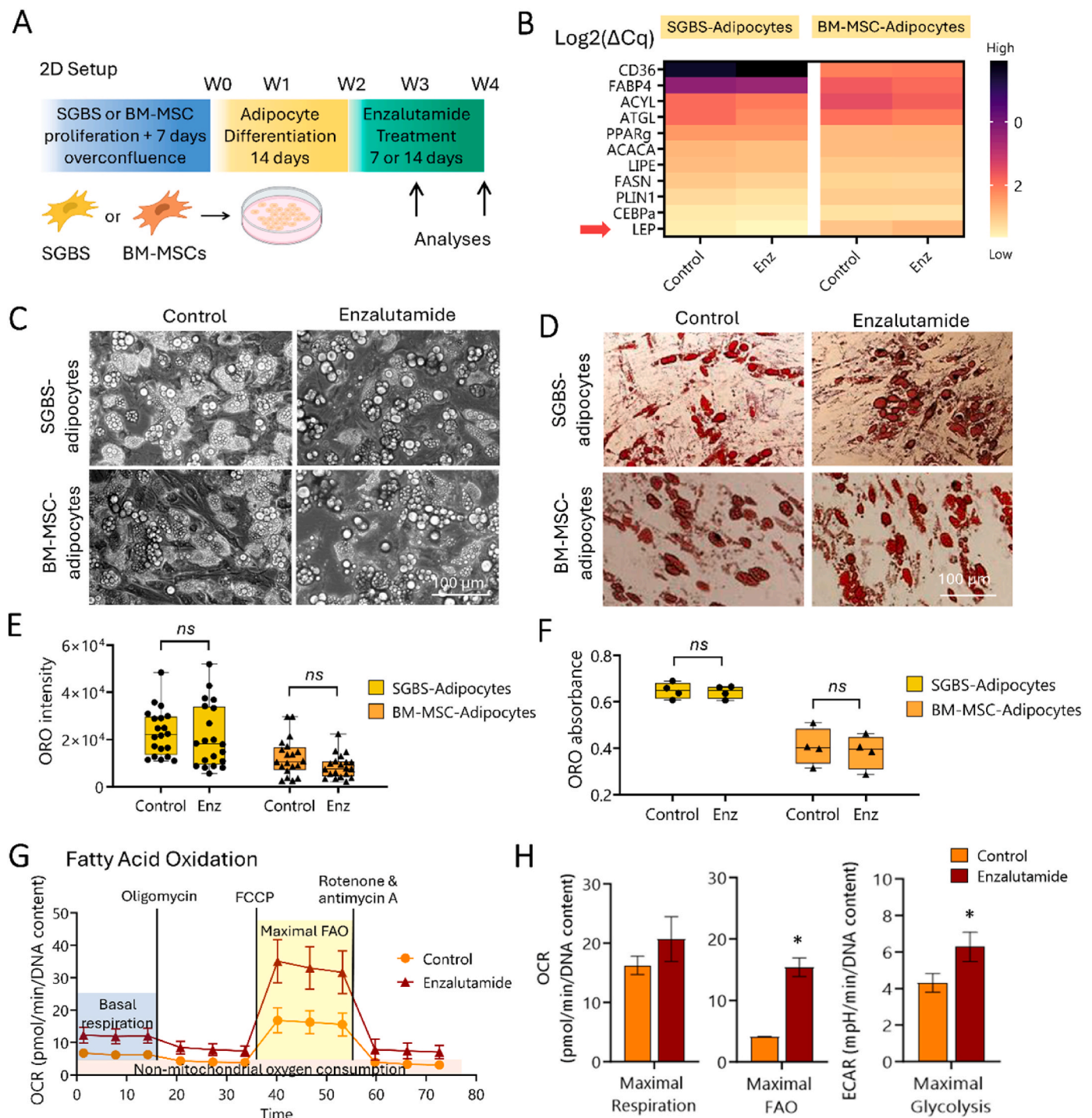
Fig. 6. Enzalutamide affects adipocyte mitochondrial respiration, fatty acid oxidation and glycolytic function. **A)** Schematic of the experimental 2D setup. **B)** mRNA levels of 2D adipocytes treated for 7 days ± Enz shown by mean Log2(ΔCq) heatmap. Black represents higher mRNA expression (i.e., lower Log2(ΔCq)) and pale yellow represents lower mRNA expression (i.e., higher Log2(ΔCq)). Results were normalized to the geomean of *7SL* and *Cyclophilin* as housekeeping genes. Enz = Enzalutamide 10 μM. **C)** Brightfield images of 2D adipocytes treated for 14 days ± Enz, with visible lipid droplet morphology change between control and Enz treatment. **D)** Brightfield images of Oil-Red-O (ORO) lipid-stained mature adipocytes after 14 days ± Enz. **E-F)** Lipid droplet quantification using (E) microscopy analysis; and (F) spectrophotometry at 520 nm following dye extraction (14 days ± Enz). Box plots shown (Median, Min, Max, *n* = 20 fields of view for E, *n* = 4 wells for F). **G-H)** Metabolic analysis after 14 days ± Enz on SGBS-derived adipocytes. Means ± SE shown, *n* = 4; G) Fatty acid oxidation (OCR = Oxygen Consumption Rate); H) Maximal mitochondrial respiration, maximal FAO (FAO = Fatty Acid Oxidation), and maximal glycolysis (ECAR = Extra Cellular Acidification Rate). Univariate general linear model, * = *p* < 0.05. Means ± SE shown, *n* = 4–7.

3.4. The presence of 3D adipocytes modifies the response of LNCaP spheroids to Enzalutamide treatment in indirect cocultures

Using the optimized GelMA-derived adipose hydrogels and indirect coculture model with PCa spheroids (See schematic in Fig. 3), we searched whether the presence of adipocytes affected the response of PCa spheroids to Enzalutamide, hypothesizing that adipocytes may reduce antiandrogen efficiency. Metabolic activity (Fig. 7A, Prestoblue
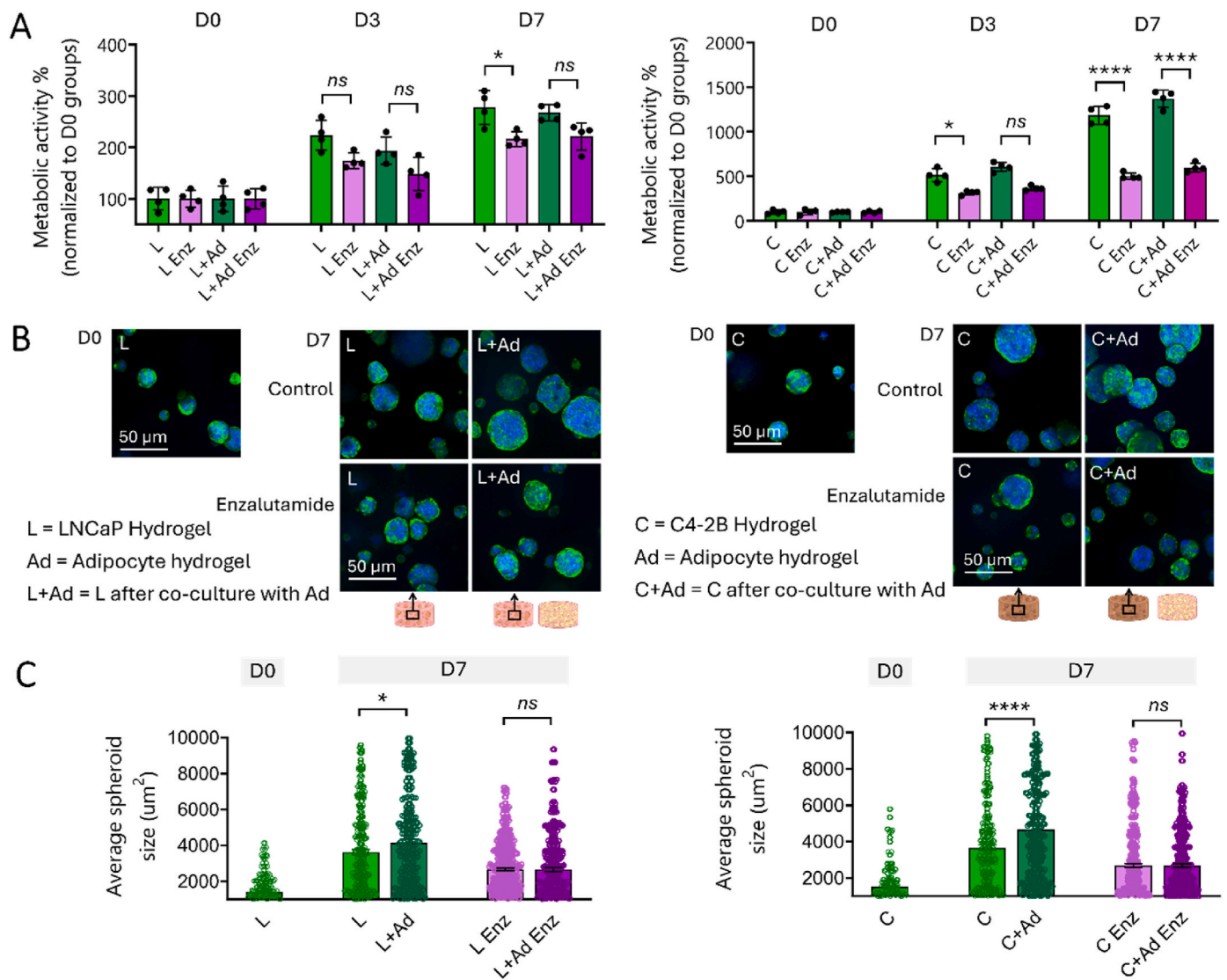
Fig. 7. **Metabolic activity and average spheroid size under Enzalutamide in adipocyte-prostate cancer cell 3D cocultures**. **A)** Metabolic activity over 7 days of cocultures ± Enz 10 µM. Means ± SD shown ($n = 4$). L: LNCaP hydrogel, C: C4-2B hydrogel, L + Ad = LNCaP hydrogel after coculture with SGBS-derived adipocyte hydrogel, C + Ad: C4-2B hydrogel after coculture with SGBS-derived adipocyte hydrogel. Enz: Enzalutamide 10 µM. **B)** Confocal images following immunofluorescence staining (Blue/DAPI = cell nuclei, green/phalloidin = actin) of GelMA hydrogels containing either LNCaP or C4-2B spheroids, ± cocultures with adipose hydrogels, ± Enz 10 µM. **C)** Average spheroid size. Means ± SE ($n = 215$–463), univariate general linear model, $* = p < 0.05$, $**** = p < 0.0001$, *ns*: non-significant.

assay) first showed that C4-2B spheroids alone responded to Enzalutamide quicker and more significantly than LNCaP spheroids alone, as can be expected as C4-2B are more metabolically active than LNCaPs (Fig. 7A right, $p < 0.0001$ versus Fig. 7A left, $p < 0.05$ at Day 7). Yet, once cocultured with the adipose microtissues, that trend stayed the same on LNCaP and C4-2B spheroids but was no longer significant on the LNCaP spheroids at day 7 (Fig. 7A, $p > 0.05$), suggesting AR-related processes may be involved in this difference. Looking at PCa spheroids upon immunofluorescence staining (Fig. 7B), followed by size analysis (Fig. 7C), we saw that without Enzalutamide, both LNCaP and C4-2B spheroids grew slightly larger in the presence of the adipose hydrogels (1.14-fold more for LNCaP spheroids, $p < 0.05$ Fig. 6C left and 1.27-fold more for C4-2B spheroids, $p < 0.0001$ Fig. 6C right), in line with the qualitative brightfield images from Fig. 4C. Yet, there were no spheroid size differences under Enzalutamide (Fig. 7C). These results mean that 1) adipocytes conferred PCa spheroids a competitive advantage (increased spheroid size) only when cocultured *without* Enzalutamide, and that 2) the presence of adipocytes affected the metabolic activity of

LNCaP spheroids, showing that adipocytes impacted cancer cells at other levels than proliferation.

At the cancer cell gene level (Fig. 8A), we looked at expression of PCa-relevant genes, i.e. prostate specific antigen *PSA* (also known as kallikrein-3 *KLK3*), and *AR* first. Both were significantly modulated. PSA was downregulated under Enzalutamide (Fig. 8B), as expected more for LNCaP than C4-2B (0.12-fold, $p < 0.001$ versus 0.6-fold, $p < 0.05$), and while this modulation was unchanged in the presence of adipocytes for LNCaP (still significant statistically, 0.16-fold, $p < 0.001$), this was no longer significant for C4-2B (0.7-fold, $p > 0.05$). *AR* was significantly increased (1.8-fold, $p < 0.05$, for LNCaP and 2.5-fold, $p < 0.001$ for C4-2B) under Enzalutamide, in line with *AR* expression under antiandrogen treatment at the start of adaptive response [23], but the presence of adipocytes did not significantly affect these values, suggesting that AR reactivation was mostly driven by antiandrogen therapy. Interestingly, we observed similar gene expression of AR variant 7 (*ARV7*) in the control group, with or without the presence of adipocytes. However, under Enzalutamide treatment, *ARV7* expression was increased in C4-2B
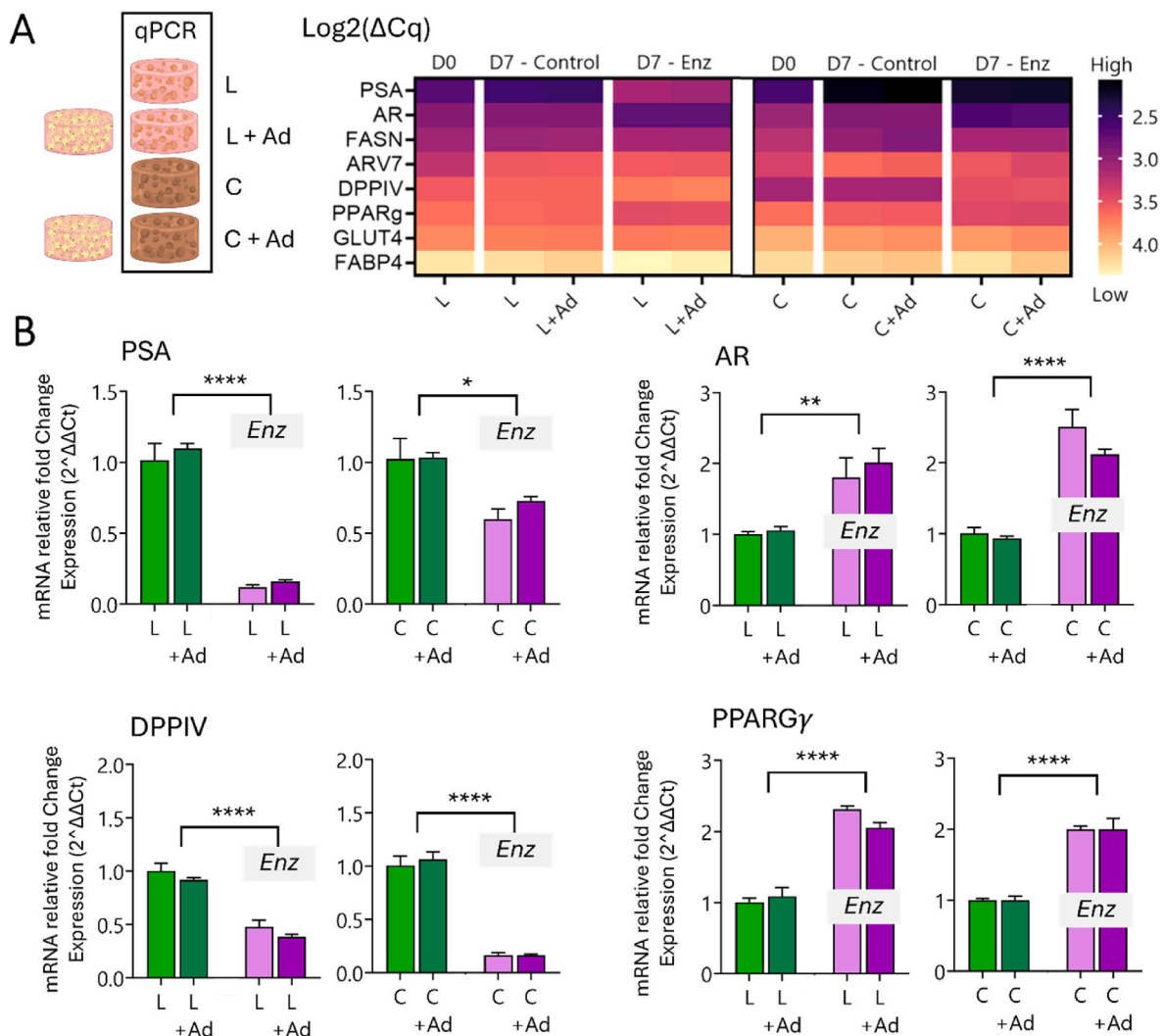
Fig. 8. Gene expression in prostate cancer cell 3D cultures ± Enzalutamide and ±adipose hydrogels. **A)** mRNA levels shown by mean Log2(*ΔCq*) heatmap, *N* = 3. **B)** mRNA relative fold changes for *PSA, AR, ARV7, DPPIV* and *PPARγ* (normalized to D7-L). Means ± standard error (SE) shown and results were normalized to the geomean of *7SL* and *RPL32* as housekeeping genes, *N* = 3. Univariate general linear model, * = *p* < 0.05, ** = *p* < 0.01, **** = *p* < 0.0001.

cells (1.7-fold), especially in the presence of adipocytes (3.3-fold), suggesting that adipocytes may contribute to Enzalutamide resistance in androgen-independent cells, as previously demonstrated [60]. However, the expression of *ARV7* from androgen-sensitive cells (LNCaP) was not affected by Enzalutamide treatment nor by the presence of adipocytes. This finding points to the potential role of adipocytes in influencing cancer cell adaptations to treatment resistance in advanced prostate cancer. Other adipocyte/cancer-relevant genes *PPARγ* and dipeptidylpeptidase 4 (*DPPIV*), known to be involved in cell-ECM interactions, were significantly altered under Enzalutamide, upregulated by 2-fold for *PPARγ* and downregulated from 0.4 to 0.2-fold for *DPPIV*. *GLUT4* and *FASN* were mostly unchanged under Enzalutamide. As expected, as a compensation mechanism to Enzalutamide pressure, *FABP4* was increased under Enzalutamide for both LNCaP and C4-2B spheroids and to a higher extent in the presence of adipocytes (Fig. 8A). However, the high number of CT values (>30 cycles), meaning little gene expression, and non-reproducibility between the three independent biological replicates, prevented any reasonable use of this information. As the integration of FFAs by cancer cells relies on FABP4, this suggests that FAPB4 was not critically contributing in this 'indirect' model system, although the presence of adipocytes did upregulate the *FABP4* gene in both LNCaP and C4-2B spheroids with and without Enzalutamide treatment.

Using nile red staining on the adipose hydrogels (Fig. 9A) and

particle analysis (Fig. 9B), we determined the number of nile red positively stained adipocytes (NR+) and lipid droplet area/cell. No significant differences in adipocytes were shown (Fig. 9B), except after coculture with LNCaP spheroids, where the number of NR + cells significantly decreased (Fig. 9B left, *p* < 0.01). As this was not seen with the AR-independent model (C4-2B spheroids), this suggests some AR-related processes which may be triggering adipocyte delipidation. Fibroblastic morphologies were observed in all adipose groups under Enzalutamide (including adipose groups alone, Fig. 9A), which suggested that Enzalutamide triggered adipocyte dedifferentiation or lipolysis [61], even in the absence of cancer cells. However, lipolysis was not confirmed by gene analysis (Fig. 9C), where typical lipolysis genes (*ATGL, LIPE, PLIN1*) remained statistically unchanged after Enzalutamide treatment. The largest differences were seen upon coculture with LNCaP with a non-significant decrease in *GLUT4* (Fig. 9D) under Enzalutamide and a significant increase in *LEP* (no Enzalutamide, *p* < 0.05) in the LNCaP/adipocytes cocultures, as could be expected for AR-responsive PCa [10]. It is also worth mentioning that *LEP* expression was similar in the adipose gels alone under Enzalutamide, as opposed to 2D adipocytes, where *LEP* was downregulated (Fig. 6B). This justifies the use of 3D models, as 2D models may be misleading the discovery of new targets.

Overall, the results suggest that a potential paracrine effect from
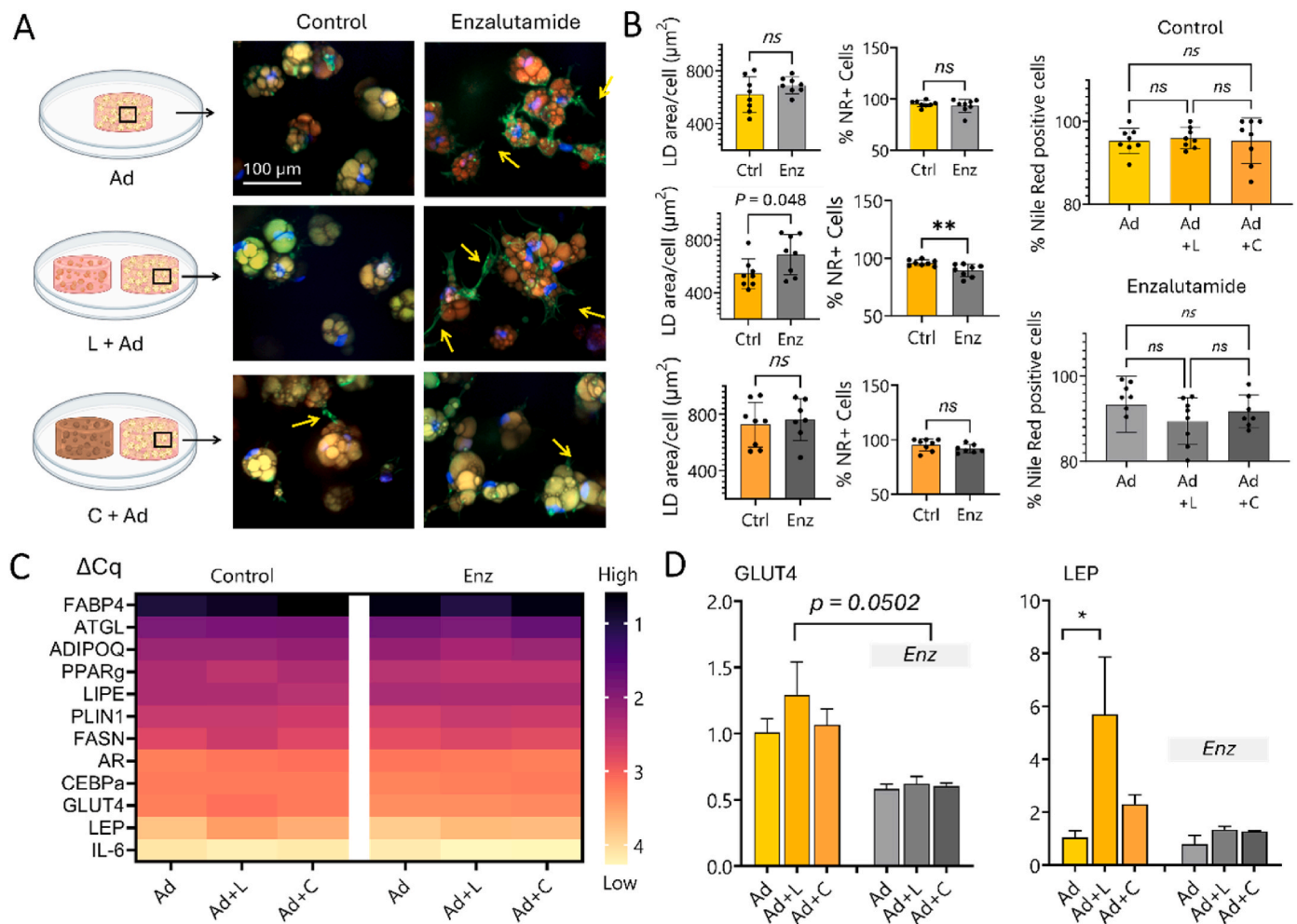
Fig. 9. Gene expression in adipose 3D cultures ± Enzalutamide and ±prostate cancer hydrogels. A-B) Schematic of cocultures and confocal images following immunofluorescence staining (Blue/DAPI = cell nuclei, green/phalloidin = actin, red/nile red = lipid droplets) of GelMA hydrogels containing SGBS-derived adipocytes, ± cocultures with LNCaP or C4-2B hydrogels, ± Enzalutamide 10 μM. Graphs show lipid droplet area per cell and percentage of nile red (NR) positive cells ± Enz 10 μM. Ctrl: Control, Enz: Enzalutamide. Means ± SD shown ($n = 7-8$), univariate general linear model, ** = $p < 0.01$, *ns*: non-significant. **C-D)** mRNA levels shown by mean *ΔCq* heatmap and mRNA relative fold changes for *GLUT4* and *LEP* (normalized to Ad) Means ± SD shown for relative fold changes and results were normalized to the geomean of *7SL* and *Cyclophilin* as housekeeping genes, $N = 3$. Heatmap legend description for C: Black represents higher mRNA expression (i.e., lower *ΔCq*) and pale yellow represents lower mRNA expression (i.e., higher *ΔCq*). L: LNCaP hydrogel, C: C4-2B hydrogel, Ad: SGBS-derived adipocyte hydrogel, L + Ad: L *after* coculture with Ad, C + Ad: C *after* coculture with Ad, Ad + L: Ad *after* coculture with L, Ad + C: Ad *after* coculture with C. Enz: Enzalutamide 10 μM. Univariate general linear model * = $p < 0.05$.

adipocytes does not compromise further the efficiency of Enzalutamide for more aggressive disease (C4-2B model, androgen independent), yet may slightly compromise efficiency for less aggressive, still androgen dependent disease (LNCaP model). This suggests an early rather than later contribution of adipocytes to adaptive response to antiandrogens, most likely involving a combination of AR and metabolic signalling, warranting further mRNA pathway analysis. In addition, adipocytes expressed less GLUT4 in the presence of Enzalutamide, which is directly linked with insulin resistance [62]. This requires further investigation as it could play a role in the metabolic syndrome observed in men under Enzalutamide, whether they have bone lesions or not [63].

4. Discussion

The need for more refined adipocyte models arises from the physical and molecular complexities of mimicking specific adipose contexts, and thereof an incomplete understanding of their implications in diseases and responses to therapies [25]. In prostate cancer, various clinical trials have demonstrated that second generation antiandrogens such as Enzalutamide have clear patient survival benefits [64] but provide

controversial reports of the effects in metastatic microenvironments [23, 65]. While such drugs initially delay metastasis to bone, antiandrogens typically lead to cancer cell and stroma adaption through AR reactivation and paracrine signalling, fuelling progression to bone [66]. Osteoblasts are an important contributor to this process, identified to be further heightened by antiandrogens [23], and bone metastasis is always present in the castration phase including antiandrogen therapy [67]. Thus, it is critical to delineate the individual and combined effects of such therapies on the other cell types of the bone tumor microenvironment for a fuller picture, including impact on the largest population in this environment, with key metabolic attributes for cancer cell survival: bone marrow adipocytes [12,59]. This is further relevant in the context of AR inhibition as key adipocyte functions, i.e., insulin signalling, lipid metabolism, fatty acid uptake, are directly impacted by androgens, with AR activation typically activating lipolysis [68].

With poorly relevant animal models (murine cells have different phenotypic makeups than human cells) and 2D human cell models displaying aberrant phenotypes, human *in vitro* 3D models provide an improved alternative [40]. GelMA is a widely used hydrogel model due to its collagen-derivative nature, innate biocompatibility, and ease of

controlled gelation. Yet, GelMA models used for mature human adipocytes are mostly derived from adipose stem cells (ASCs) [41,69–73] or use extracted adipocytes [69,71] from subcutaneous fat, which limits physiological relevance when studying metabolically dysregulated metastatic microenvironments. To our knowledge, our group has been the only one to date to use GelMA for adipocytes from human pre-adipocytes in the form of SGBS cells [32,33], which provided adipocyte model variety for increased scope and relevance. BM-MSCs in GelMA for adipogenesis is also underused [32,33,74], yet should be further considered for bone-related investigations considering the differences between white and bone marrow adipocytes presented in this study. Most ASC-derived adipose GelMA gels showed that 5 % w/v concentrations were more favourable to adipogenesis compared to 10 % or 15 % [73,75], which was in line here with softer GelMA hydrogels for BM-MSC- and SGBS-derived adipocytes (4 %, 3 kPa). This result may also be due to an increase in viscoelastic changes over time in terms of stress relaxation increasing progressively more in adipose hydrogels from lower GelMA concentrations, as previously measured by mathematical modelling [75]. With cells changing the percentage of stress relaxation, the transformation of cell-loaded hydrogels into a more fluid-like environment generates a more favourable adipogenic response [75]. This may be partially mediated by promotion of the CAV1-YAP axis, as seen in the enhanced adipogenesis of BM-MSCs in softer (0.5 kPa) versus stiffer (23.4 kPa) environments in a prior study in GelMA [74].

Methacrylated hyaluronic acid (HAMA) is often combined with GelMA to drive chondrogenesis [76]. Hyaluronic acid, an important extracellular matrix (ECM) component of the tumor microenvironment has been reported to be elevated in primary and metastatic tumor tissues, including 75–80 % in prostate tissues [77]. When used with GelMA in ASC-derived adipose hydrogels, comparing GelMA and GelMA/-HAMA (referred to HyaMA in that study [73]), gene expression was similar, such as seen in our study for both cell types, but there was no comparison of lipid content nor mechanical comparison between the gels as done here. Our study provided evidence that at similar mechanical stiffness (HAMA-1% versus GelMA-1%/HAMA-1%), the presence of HAMA in the combination group decreased lipid content. Most genes were similar between those two groups, but *LEP* was the only gene which decreased over the 3 weeks of differentiation (and in all HAMA groups). This result is likely due to reduced lipid formation for HAMA groups as *LEP* is regulated by a fat-sensing noncanonical PPARγ/RXRα-binding sequence transduction pathway, and *LEP* expression increases with lipid content in adipocytes [78], which we directly observed here. Although our results showed that HAMA is detrimental to *LEP* expression and lipid content, compared to HAMA/-GelMA at same stiffness, differences in viscoelasticity cannot be fully excluded and warrants further investigation, as HA-based hydrogels are typically favourable to adipocyte functions [42].

Our study further demonstrated how the origin of cells (WAT or BMAT) led to genetic and phenotypic differences under antiandrogen treatment, and in coculture, that may critically impact result interpretation. The use of SGBS-derived adipose models may be more relevant than ASC-derived adipose models to study the specific impact of white adipocytes in advanced PCa metastatic lesions other than bone (i.e, visceral, lymph nodes, liver, lungs) in the context of androgen deprivation. Such models may better mimic metabolic dysregulations compared to healthy ASC-derived adipose models. SGBS cells are remarkable as they can be used up to 50 population doublings (as opposed to no more than 5 typically for human stem cells), without immortalization [52]. SGBS-derived adipocytes are robustly expressing mature human adipocyte profiles, yet are more sensitive to metabolic variations [79]. They have increased insulin sensitivity, with high levels of the insulin-dependent glucose transporter (GLUT4), glucose uptake and activation of the insulin receptor signaling pathway [79], which is more relevant in the context of androgen deprivation and metabolic syndrome of men with advanced prostate cancer [80]. Here, their ability

to alter lipid metabolism with PCa spheroids (*FABP4* upregulation [57], lipid content decrease) under antiandrogens in the 3D models compared to 2D culture, reinforced the concept of 3D models being more physiologically relevant [40]. Limitations of 3D hydrogel models include the lack of options for in depth metabolic analysis which still warrants 2D models. Here, a seahorse assay enabled to pinpoint Enzalutamide as causing increase in mitochondrial respiration, fatty acid oxidation, the catabolism of fatty acids and glycolysis and the catabolism of glucose, suggesting that Enzalutamide-treated adipocytes were able to generate more energy [79]. This could be correlated with the altered lipid metabolism in 3D cocultures and under Enzalutamide. Having an increased energy production caused by Enzalutamide is a concern, as this may potentially have detrimental consequences by priming permissive premetastatic niches in adipose-containing locations in the body, for more successful PCa cell homing and/or proliferation [81] and warrants further investigation.

Antiandrogens are linked to metabolic syndrome, including increased fat accumulation in men, changes in lipid profiles and insulin resistance [80]. Human adipocytes express *AR*, respond to testosterone with a decrease in leptin expression, unaffected adiponectin levels [82] but inhibition of phosphorylation of AMPK [83]. Here we have shown how AR targeting via Enzalutamide directly increased *AR* expression in PCa microtissues. Interestingly, although LNCaP and C4-2B cells do not naturally express *ARV7*, or do express low levels at the transcriptional level only [84,85], we observed that under Enzalutamide treatment, *ARV7* expression was significantly increased in C4-2B cells, particularly in the presence of adipocytes. ARV7 is a crucial androgen receptor variant that plays a significant role in the development of resistance to Enzalutamide [60]. Despite the increase in *ARV7* expression, this did not lead to significantly higher spheroid growth, suggesting that the upregulation of *ARV7* in this context may not be sufficient to drive aggressive tumor growth at early stages. The paracrine effects of adipocytes in indirect cocultures did not cause such dysregulation, although it tentatively upregulated *FABP4*, a transporter with which facilitates lipid uptake and regulates free fatty acid content inside cell bodies, in line with previous reports [57]. This is critically relevant to cancer where FABP4 protein release from adipocytes can be taken up by PCa cells as an energy source [7], demonstrating exacerbated adipocyte contribution to the adaptive response following antiandrogen treatment, especially on AR-dependent tumor cells (LNCaP). *FABP4* increase under Enzalutamide was correlated with lipid size decrease in both 2D and 3D, although it was significant only for 3D adipocytes cocultured with LNCaP. Both *FABP4* upregulation and lipid content decrease under Enzalutamide in coculture are in line with increased lipid metabolism and lipolysis [86] and could be correlated with a stronger effect on early stage metastasis where full AR independence has not been established yet. This is in line with a previous study where a significant tumor-promoting effect of white murine adipocytes was observed only in highly differentiated, AR-dependent cancer cells while there was no adipocyte effect on AR-independent cell lines [86]. It must be noted that opposite results were also reported [87,88], showing that there are still controversies about the role of adipocytes and their secreted adipokines in AR-related cancers. Interestingly, the typical upregulation of LEP in the presence of cancer (seen here too) was not observed under Enzalutamide, and *GLUT4* was downregulated even without the PCa microtissues. This is an important result as *GLUT4* expression in adipocytes is linked with metabolic dysfunctions, impacting insulin signaling pathways and glucose uptake efficiency [62].

While unraveling novel important results of adipocyte-prostate cancer behaviors under Enzalutamide, limitations of the models include the lack of osteoblasts, which is known to be key in the crosstalk with cancer cells and resistance to Enzalutamide in metastatic microenvironments [89]. For instance, *DPPIV* is already known to be elevated in primary disease [90], yet here *DPPIV* was reduced under Enzalutamide. As we proved previously that *DPPIV* was indeed upregulated in the presence of osteoblasts in a mineralized matrix 3D model [23] and

aligned with clinical findings [91], this calls for opting for a triple coculture models in future investigations. We have previously shown that the same hydrogel system (GelMA 4 %) could be used to derive mineralized tissues [32], facilitating future investigations. Another limitation is the indirect coculture model which may limit the crosstalk between cancer cells and adipocytes, potentially masking important, yet less expressed, molecular pathways. While direct cocultures, and enhanced proximity between adipocytes and cancer cells, may be physiologically relevant and lead to more discoveries [19], difficulties still arise in terms of successful co-encapsulation of viable cells of mature phenotype, imaging and the determination of individual cell population contributions [32]. While these studies are beyond the scope of the current work, our results suggested that the choice of adipocytes (from WAT or BMAT) had a significant influence on the phenotypic makeup of mature adipocytes and response to Enzalutamide alone and in the presence of AR-dependent cancer cells. Their successful culture in 3D hydrogel models enabled to identify altered lipid metabolism mechanisms and introduced human adipocytes as an additional source of antiandrogen resistance in mCRPC.

CRediT authorship contribution statement

Agathe Bessot: Writing – review & editing, Methodology, Investigation, Formal analysis, Data curation, Conceptualization. **Joan Röhl:** Writing – review & editing, Formal analysis, Data curation. **Maria Emmerich:** Writing – review & editing, Visualization, Methodology, Investigation, Formal analysis, Data curation. **Anton Klotz:** Writing – review & editing, Investigation, Formal analysis. **Akhilandeshwari Ravichandran:** Writing – review & editing, Visualization, Methodology, Investigation, Formal analysis, Data curation. **Christoph Meinert:** Methodology. **David Waugh:** Supervision, Funding acquisition. **Jacqui McGovern:** Supervision. **Jenni Gunter:** Supervision, Methodology, Investigation. **Nathalie Bock:** Writing – review & editing, Writing – original draft, Visualization, Validation, Supervision, Software, Resources, Project administration, Methodology, Investigation, Funding acquisition, Formal analysis, Data curation, Conceptualization.

Data and materials availability

All data needed to evaluate the conclusions are presented in the publication. Additional data related to this publication may be requested from N.B. directly.

Funding

Declaration of competing interest

The authors declare the following financial interests/personal relationships which may be considered as potential competing interests: Christoph Meinert is a shareholder, Executive Director, and the CEO of Gelomics Pty Ltd. The other authors declare that they have no competing interests.

Appendix A. Supplementary data

Supplementary data to this article can be found online at https://doi.org/10.1016/j.mtbio.2024.101424.

References

[1] R.J. De Berardinis, N.S. Chandel, Fundamentals of cancer metabolism, Sci. Adv. 2 (2016).

[2] B. Faubert, A. Solmonson, R.J. DeBerardinis, Metabolic reprogramming and cancer progression, Science (2020) 368.

[3] N.N. Pavlova, C.B. Thompson, The emerging hallmarks of cancer metabolism, Cell Metab. 23 (2016) 27–47.

[4] K.M. Nieman, I.L. Romero, B. Van Houten, E. Lengyel, Adipose tissue and adipocytes support tumorigenesis and metastasis, Biochim. Biophys. Acta-Molecular Cell Biol. Lipids 1831 (2013) 1533–1541, https://doi.org/10.1016/j.bbalip.2013.02.010.

[5] K.I. Avgerinos, N. Spyrou, C.S. Mantzoros, M. Dalamaga, Obesity and cancer risk: emerging biological mechanisms and perspectives, Metabolism 92 (2019) 121–135.

[6] G.A. Colditz, L.L. Peterson, Obesity and cancer: evidence, impact, and future directions, Clin. Chem. 64 (2018) 154–162, https://doi.org/10.1373/clinchem.2017.277376.

[7] H. Uehara, T. Kobayashi, M. Matsumoto, S. Watanabe, A. Yoneda, Y. Bando, Adipose tissue : critical contributor to the development of prostate cancer, J. Med. Investig. 65 (2018) 9–17.

[8] M.R. Reagan, C.J. Rosen, Navigating the bone marrow niche: translational insights and cancer-driven dysfunction, Nat. Rev. Rheumatol. 12 (2016) 154–168, https://doi.org/10.1038/nrrheum.2015.160.

[9] P. Hardouin, T. Rharass, S. Lucas, Bone marrow adipose tissue: to Be or not to Be a typical adipose tissue? Front. Endocrinol. 7 (2016) 85, https://doi.org/10.3389/fendo.2016.00085.

[10] K.J. Suchacki, A.A.S. Tavares, D. Mattiucci, E.L. Scheller, G. Papanastasiou, C. Gray, M.C. Sinton, L.E. Ramage, W.A. McDougald, A. Lovdel, et al., Bone marrow adipose tissue is a unique adipose subtype with distinct roles in glucose homeostasis, Nat. Commun. 11 (2020) 1–18, https://doi.org/10.1038/s41467-020-16878-2.

[11] A. Hardaway, M. Herroon, E. Rajagurubandara, I. Podgorski, Bone marrow fat: linking adipocyte-induced inflammation with skeletal metastases, Cancer Metastasis Rev. (2014) 1–17, https://doi.org/10.1007/s10555-013-9484-y.

[12] E.V. Morris, C.M. Edwards, Bone marrow adipose tissue: a new player in cancer metastasis to bone, Front. Endocrinol. 7 (2016) 90, https://doi.org/10.3389/fendo.2016.00090.

[13] A.L. Hardaway, M.K. Herroon, E. Rajagurubandara, I. Podgorski, Marrow adipocyte-derived CXCL1 and CXCL2 contribute to osteolysis in metastatic prostate cancer, Clin. Exp. Metastasis 32 (2015) 353–368, https://doi.org/10.1007/s10585-015-9714-5.

[14] B.M. Abdallah, Marrow adipocytes inhibit the differentiation of mesenchymal stem cells into osteoblasts via suppressing BMP-signaling, J. Biomed. Sci. 24 (2017) 1–10, https://doi.org/10.1186/s12929-017-0321-4.

[15] S. Muruganandan, A.M. Ionescu, C.J. Sinal, At the crossroads of the adipocyte and osteoclast differentiation programs: future therapeutic perspectives, Int. J. Mol. Sci. 21 (2020) 2277.

[16] G. Luo, M. Tang, Q. Zhao, L. Lu, Y. Xie, Y. Li, C. Liu, L. Tian, X. Chen, X. Yu, Bone marrow adipocytes enhance osteolytic bone destruction by activating 1q21.3 (S100A7/8/9-IL6R)-TLR4 pathway in lung cancer, J. Cancer Res. Clin. Oncol. 146 (2020) 2241–2253, https://doi.org/10.1007/s00432-020-03277-9.

[17] J. Li, J. Wu, Y. Xie, X. Yu, Bone marrow adipocytes and lung cancer bone metastasis: unraveling the role of adipokines in the tumor microenvironment, Front. Oncol. 14 (2024) 1360471.

[18] E. Shin, J.S. Koo, The role of adipokines and bone marrow adipocytes in breast cancer bone metastasis, Int. J. Mol. Sci. 21 (2020) 1–21.

[19] J.G. Kwak, J. Lee, Bone marrow adipocytes contribute to tumor microenvironment-driven chemoresistance via sequestration of doxorubicin, Cancers 15 (2023), https://doi.org/10.3390/cancers15102737.

[20] M.K. Herroon, J.D. Diedrich, E. Rajagurubandara, C. Martin, K.R. Maddipati, S. Kim, E.I. Heath, J. Granneman, I. Podgorski, Prostate tumor cell-derived IL1β induces an inflammatory phenotype in bone marrow adipocytes and reduces sensitivity to docetaxel via lipolysis-dependent mechanisms, Mol. Cancer Res. 17 (2019) 2508–2521, https://doi.org/10.1158/1541-7786.MCR-19-0540.

[21] J.J. Body, S. Casimiro, L. Costa, Targeting bone metastases in prostate cancer: improving clinical outcome, Nat. Rev. Urol. 12 (2015) 340–356, https://doi.org/10.1038/nrurol.2015.90.

[22] A.J. Armstrong, M. Al-Adhami, P. Lin, T. Parli, J. Sugg, J. Steinberg, B. Tombal, C.N. Sternberg, J. De Bono, H.I. Scher, et al., Association between new unconfirmed bone lesions and outcomes in men with metastatic castration-resistant prostate cancer treated with enzalutamide: secondary analysis of the PREVAIL and AFFIRM randomized clinical trials, in: Proceedings of the JAMA Oncology, American Medical Association, 2020, pp. 217–225, 6.

[23] N. Bock, T. Kryza, A. Shokoohmand, J. Röhl, A. Ravichandran, M.L. Wille, C.C. Nelson, D.W. Hutmacher, J.A. Clements, In vitro engineering of a bone metastases model allows for study of the effects of antiandrogen therapies in advanced prostate cancer, Sci. Adv. 7 (2021), https://doi.org/10.1126/sciadv.abg2564.

[24] Y. Kong, L. Cheng, F. Mao, Z. Zhang, Y. Zhang, E. Farah, J. Bosler, Y. Bai, N. Ahmad, S. Kuang, et al., Inhibition of cholesterol biosynthesis overcomes enzalutamide resistance in castration-resistant prostate cancer (CRPC) X, J. Biol. Chem. 293 (2018) 14328–14341, https://doi.org/10.1074/jbc.RA118.004442.

[25] C.S. Murphy, L. Liaw, M.R. Reagan, In vitro tissue-engineered adipose constructs for modeling disease, BMC Biomed. Eng. 1 (2019), https://doi.org/10.1186/s42490-019-0027-7.

[26] M. Rebeaud, C. Bouche, S. Dauvillier, C. Attané, C. Arellano, C. Vaysse, F. Fallone, C. Muller, A novel 3D culture model for human primary mammary adipocytes to study their metabolic crosstalk with breast cancer in lean and obese conditions, Sci. Rep. 13 (2023) 4707, https://doi.org/10.1038/s41598-023-31673-x.

[27] H. Horder, M.G. Lasheras, N. Grummel, A. Nadernezhad, J. Herbig, S. Ergün, J. Teßmar, J. Groll, B. Fabry, P. Bauer-Kreisel, et al., Bioprinting and differentiation of adipose-derived stromal cell spheroids for a 3d breast cancer-adipose tissue model, Cells 10 (2021) 803, https://doi.org/10.3390/cells10040803.

[28] S. Das, F. Pati, Y.J. Choi, G. Rijal, J.H. Shim, S.W. Kim, A.R. Ray, D.W. Cho, S. Ghosh, Bioprintable, cell-laden silk fibroin-gelatin hydrogel supporting multilineage differentiation of stem cells for fabrication of three-dimensional tissue constructs, Acta Biomater. 11 (2015) 233–246, https://doi.org/10.1016/j.actbio.2014.09.023.

[29] R.D. Abbott, W.K. Raja, R.Y. Wang, J.A. Stinson, D.L. Glettig, K.A. Burke, D.L. Kaplan, Long term perfusion system supporting adipogenesis, Methods 84 (2015) 84–89, https://doi.org/10.1016/j.ymeth.2015.03.022.

[30] H. Fairfield, C. Falank, M. Farrell, C. Vary, J.M. Boucher, H. Driscoll, L. Liaw, C.J. Rosen, M.R. Reagan, Development of a 3D bone marrow adipose tissue model, Bone (2018), https://doi.org/10.1016/j.bone.2018.01.023.

[31] P. Vidyasekar, P. Shyamsunder, S.K. Sahoo, R.S. Verma, Scaffold-free and scaffold-assisted 3D culture enhances differentiation of bone marrow stromal cells, Vitr. Cell. Dev. Biol. - Anim. 52 (2016) 204–217, https://doi.org/10.1007/s11626-015-9971-2.

[32] A. Bessot, J. Gunter, D. Waugh, J.A. Clements, D.W. Hutmacher, J. McGovern, N. Bock, GelMA and biomimetic culture allow the engineering of mineralized, adipose, and tumor tissue human microenvironments for the study of advanced prostate cancer in vitro and in vivo, Adv. Healthc. Mater. (2023) 2201701, https://doi.org/10.1002/adhm.202201701.

[33] A. Ravichandran, C. Meinert, O. Bas, D.W. Hutmacher, N. Bock, Engineering a 3D bone marrow adipose composite tissue loading model suitable for studying mechanobiological questions, Mater. Sci. Eng. C 128 (2021) 112313, https://doi.org/10.1016/j.msec.2021.112313.

[34] E. Mosaad, K. Chambers, K. Futrega, J. Clements, M.R. Doran, Using high throughput microtissue culture to study the difference in prostate cancer cell behavior and drug response in 2D and 3D co-cultures, BMC Cancer 18 (2018) 592, https://doi.org/10.1186/s12885-018-4473-8.

[35] H. Fairfield, C. Falank, M. Farrell, C. Vary, J.M. Boucher, H. Driscoll, L. Liaw, C.J. Rosen, M.R. Reagan, Development of a 3D bone marrow adipose tissue model, Bone 118 (2019) 77–88, https://doi.org/10.1016/j.bone.2018.01.023.

[36] H. Fairfield, R. Condruti, M. Farrell, R. Di Iorio, C.A. Gartner, C. Vary, M.R. Reagan, Development and characterization of three cell culture systems to investigate the relationship between primary bone marrow adipocytes and myeloma cells, Front. Oncol. 12 (2023) 912834, https://doi.org/10.3389/fonc.2022.912834.

[37] R.D. Hume, L. Berry, S. Reichelt, M. D'Angelo, J. Gomm, R.E. Cameron, C.J. Watson, An engineered human adipose/collagen model for in vitro breast cancer cell migration studies, Tissue Eng. - Part A 24 (2018) 1309–1319, https://doi.org/10.1089/ten.tea.2017.0509.

[38] L. Bougaret, L. Delort, H. Billard, C. Le Huede, C. Boby, A. De la Foye, A. Rossary, A. Mojallal, O. Damour, C. Auxenfans, et al., Adipocyte/breast cancer cell crosstalk in obesity interferes with the anti-proliferative efficacy of tamoxifen, PLoS One 13 (2018), https://doi.org/10.1371/journal.pone.0191571.

[39] W. Jiao, J. Shan, X. Gong, Y. Sun, L. Sang, X. Ding, H. Zhou, M. Yu, GelMA hydrogel: a game-changer in 3D tumor modeling, Mater. Today Chem. 38 (2024) 102111.

[40] L.J. Bray, D.W. Hutmacher, N. Bock, Addressing patient specificity in the engineering of tumor models, Front. Bioeng. Biotechnol. 7 (2019) 217, https://doi.org/10.3389/fbioe.2019.00217.

[41] B. O'Donnell, S. Al-Ghadban, C. Ives, C. M. L'Ecuyer, T. Monjure, M. Romero-Lopez, Z. Li, S. Goodman, H. Lin, R. Tuan, et al., Adipose tissue-derived stem cells retain their adipocyte differentiation potential in three-dimensional hydrogels and bioreactors, Biomolecules 10 (2020) 1070, https://doi.org/10.3390/biom10071070.

[42] K.M. Tharp, A. Stahl, Bioengineering beige adipose tissue therapeutics, Front. Endocrinol. 6 (2015) 167373.

[43] Y. Quan, J. Li, J. Cai, Y. Liao, Y. Zhang, F. Lu, Transplantation of beige adipose organoids fabricated using adipose acellular matrix hydrogel improves metabolic dysfunction in high-fat diet-induced obesity and type 2 diabetes mice, J. Cell. Physiol. 239 (2024) e31191, https://doi.org/10.1002/jcp.31191.

[44] P.A. Levett, F.P.W. Melchels, K. Schrobback, D.W. Hutmacher, J. Malda, T.J. Klein, A biomimetic extracellular matrix for cartilage tissue engineering centered on photocurable gelatin, hyaluronic acid and chondroitin sulfate, Acta Biomater. 10 (2014) 214–223.

[45] D. Loessner, C. Meinert, E. Kaemmerer, L.C. Martine, K. Yue, P.A. Levett, T.J. Klein, F.P.W. Melchels, A. Khademhosseini, D.W. Hutmacher, Functionalization, preparation and use of cell-laden gelatin methacryloyl-based hydrogels as modular tissue culture platforms, Nat. Protoc. 11 (2016) 727–746, https://doi.org/10.1038/nprot.2016.037.

[46] S. Bhatia, E.W. Thompson, J.H. Gunter, Studying the metabolism of epithelial-mesenchymal plasticity using the seahorse XFe96 extracellular flux analyzer, in: Methods in Molecular Biology, Humana Press Inc., 2020, pp. 327–340, 2179.

[47] C. Zhao, Z. Zhang, X. Hu, L. Zhang, Y. Liu, Y. Wang, Y. Guo, T. Zhang, W. Li, B. Li, Hyaluronic acid correlates with bone metastasis and predicts poor prognosis in small-cell lung cancer patients, Front. Endocrinol. 12 (2022) 785192, https://doi.org/10.3389/fendo.2021.785192.

[48] K.H. Chang, H.T. Liao, J.P. Chen, Preparation and characterization of gelatin/hyaluronic acid cryogels for adipose tissue engineering: in vitro and in vivo studies, Acta Biomater. 9 (2013) 9012–9026, https://doi.org/10.1016/j.actbio.2013.06.046.

[49] P.A. Levett, D.W. Hutmacher, J. Malda, T.J. Klein, Hyaluronic acid enhances the mechanical properties of tissue-engineered cartilage constructs, PLoS One 9 (2014) e113216, https://doi.org/10.1371/journal.pone.0113216.

[50] C.S. Murphy, L. Liaw, M.R. Reagan, In vitro tissue-engineered adipose constructs for modeling disease, BMC Biomed. Eng. 1 (2019) 27, https://doi.org/10.1186/s42490-019-0027-7.

[51] K. Yue, G. Trujillo-de Santiago, M.M. Alvarez, A. Tamayol, N. Annabi, A. Khademhosseini, Synthesis, properties, and biomedical applications of gelatin methacryloyl (GelMA) hydrogels, Biomaterials 73 (2015) 254–271, https://doi.org/10.1016/J.BIOMATERIALS.2015.08.045.

[52] P. Fischer-Posovszky, F.S. Newell, M. Wabitsch, H.E. Tornqvist, Human SGBS cells - a unique tool for studies of human fat cell biology, Obes. Facts 1 (2008) 184–189.

[53] H. Fairfield, S. Costa, C. Falank, M. Farrell, C.S. Murphy, A. D'Amico, H. Driscoll, M.R. Reagan, Multiple myeloma cells alter adipogenesis, increase senescence-related and inflammatory gene transcript expression, and alter metabolism in preadipocytes, Front. Oncol. 10 (2021) 1, https://doi.org/10.3389/fonc.2020.584683.

[54] M.K. Herroon, J.D. Diedrich, I. Podgorski, New 3D-culture approaches to study interactions of bone marrow adipocytes with metastatic prostate cancer cells, Front. Endocrinol. 7 (2016) 84, https://doi.org/10.3389/fendo.2016.00084.

[55] B. Dirat, L. Bochet, M. Dabek, D. Daviaud, S. Dauvillier, B. Majed, Y.Y. Wang, A. Meulle, B. Salles, S. Le Gonidec, et al., Cancer-associated adipocytes exhibit an activated phenotype and contribute to breast cancer invasion, Cancer Res. 71 (2011) 2455–2465, https://doi.org/10.1158/0008-5472.CAN-10-3323.

[56] C.M.L. Fontana, M.E. Maselli, R.F.P. Elizalde, N.A.D. Monaco, A.L.U. Recupero, J.D.L. Laur, Leptin increases prostate cancer aggressiveness, J. Physiol. Biochem. 67 (2011) 531–538, https://doi.org/10.1007/s13105-011-0098-y.

[57] M.K. Herroon, E. Rajagurubandara, A.L. Hardaway, K. Powell, A. Turchick, D. Feldmann, I. Podgorski, Bone marrow adipocytes promote tumor growth in bone via FABP4-dependent mechanisms, Oncotarget 4 (2013) 2108–2123.

[58] C. Attané, C. Muller, Drilling for Oil: tumor-surrounding adipocytes fueling cancer, Trends in Cancer 6 (2020) 593–604.

[59] G.J. Luo, Y.D. He, X.J. Yu, Bone marrow adipocyte: an intimate partner with tumor cells in bone metastasis, Front. Endocrinol. 9 (2018) 14, https://doi.org/10.3389/fendo.2018.00339.

[60] Z. Zheng, J. Li, Y. Liu, Z. Shi, Z. Xuan, K. Yang, C. Xu, Y. Bai, M. Fu, Q. Xiao, et al., The crucial role of AR-V7 in enzalutamide-resistance of castration-resistant prostate cancer, Cancers 14 (2022) 4877, https://doi.org/10.3390/CANCERS14194877.

[61] M. Ahmadian, Y. Wang, H.S. Sul, Lipolysis in adipocytes, Int. J. Biochem. Cell Biol. 42 (2010) 555–559.

[62] M. Hernandez, S. Shin, C. Muller, C. Attané, The role of bone marrow adipocytes in cancer progression: the impact of obesity, Cancer Metastasis Rev. 41 (2022) 589–605.

[63] E. Gómez-Gómez, J. Carrasco-Valiente, J.P. Campos-Hernández, A.M. Blanca-Pedregosa, J.M. Jiménez-Vacas, J. Ruiz-García, J. Valero-Rosa, R.M. Luque, M.J. Requena-Tapia, Clinical association of metabolic syndrome, C-reactive protein and testosterone levels with clinically significant prostate cancer, J. Cell Mol. Med. 23 (2019) 934–942, https://doi.org/10.1111/jcmm.13994.

[64] H.I. Scher, K. Fizazi, F. Saad, M.-E. Taplin, C.N. Sternberg, K. Miller, R. de Wit, P. Mulders, K.N. Chi, N.D. Shore, et al., Increased survival with enzalutamide in prostate cancer after chemotherapy, N. Engl. J. Med. 367 (2012) 1187–1197, https://doi.org/10.1056/nejmoa1207506.

[65] C.W. Jeong, J.H. Han, D.D. Kwon, J.Y. Joung, C.-S. Kim, H. Ahn, J.H. Hong, T.-H. Kim, B.H. Chung, S.S. Jeon, et al., Oncological outcomes in men with metastatic castration-resistant prostate cancer treated with enzalutamide with versus without confirmatory bone scan, Cancer Res. Treat. 56 (2024) 634–641, https://doi.org/10.4143/crt.2023.848.

[66] J.J. Yin, Y.N. Liu, H. Tillman, B. Barrett, S. Hewitt, K. Ylaya, L. Fang, R. Lake, E. Corey, C. Morrissey, et al., AR-regulated TWEAK-FN14 pathway promotes prostate cancer bone metastasis, Cancer Res. 74 (2014) 4306–4317, https://doi.org/10.1158/0008-5472.CAN-13-3233.

[67] X. Zhang, Interactions between cancer cells and bone microenvironment promote bone metastasis in prostate cancer, Cancer Commun. 39 (2019) 1–10.

[68] M.W. O'Reilly, P.J. House, J.W. Tomlinson, Understanding androgen action in adipose tissue, J. Steroid Biochem. Mol. Biol. 143 (2014) 277–284.

[69] F.B. Albrecht, F.F. Schmidt, A.C. Volz, P.J. Kluger, Bioprinting of 3D adipose tissue models using a GelMA-bioink with human mature adipocytes or human adipose-derived stem cells, Gels 8 (2022) 611, https://doi.org/10.3390/gels8100611.

[70] J. Colle, P. Blondeel, A. De Bruyne, S. Bochar, L. Tytgat, C. Vercruysse, S. Van Vlierberghe, P. Dubruel, H. Declercq, Bioprinting predifferentiated adipose-derived mesenchymal stem cell spheroids with methacrylated gelatin ink for adipose tissue engineering, J. Mater. Sci. Mater. Med. 31 (2020) 1–15, https://doi.org/10.1007/s10856-020-06374-w.

[71] B. Huber, K. Borchers, G.E.M. Tovar, P.J. Kluger, Methacrylated gelatin and mature adipocytes are promising components for adipose tissue engineering, J. Biomater. Appl. 30 (2016) 699–710, https://doi.org/10.1177/0885328215587450.

[72] L. Tytgat, L. Van Damme, J. Van Hoorick, H. Declercq, H. Thienpont, H. Ottevaere, P. Blondeel, P. Dubruel, S. Van Vlierberghe, Additive manufacturing of photo-crosslinked gelatin scaffolds for adipose tissue engineering, Acta Biomater. 94 (2019) 340–350, https://doi.org/10.1016/j.actbio.2019.05.062.

[73] L. Kessler, S. Gehrke, M. Winnefeld, B. Huber, E. Hoch, T. Walter, R. Wyrwa, M. Schnabelrauch, M. Schmidt, M. Kuckelhaus, et al., Methacrylated gelatin/hyaluronan-based hydrogels for soft tissue engineering, J. Tissue Eng. 8 (2017) 1–14, https://doi.org/10.1177/2041731417744157.

[74] S. Xiang, Z. Li, M.R. Fritch, L. Li, S. Velankar, Y. Liu, J. Sohn, N. Baker, H. Lin, R. S. Tuan, Caveolin-1 mediates soft scaffold-enhanced adipogenesis of human mesenchymal stem cells, Stem Cell Res. Ther. 12 (2021), https://doi.org/10.1186/s13287-021-02356-z.

[75] F.D. Martinez-Garcia, M.M. Valk, P.K. Sharma, J.K. Burgess, M.C. Harmsen, Adipose tissue-derived stromal cells alter the mechanical stability and viscoelastic properties of gelatine methacryloyl hydrogels, Int. J. Mol. Sci. 22 (2021) 10153, https://doi.org/10.3390/ijms221810153.

[76] Y.O. Waidi, I. Kariim, S. Datta, Bioprinting of gelatin-based materials for orthopedic application, Front. Bioeng. Biotechnol. 12 (2024) 1357460.

[77] Y. Hao, A.B. Zerdoum, A.J. Stuffer, A.K. Rajasekaran, X. Jia, Biomimetic hydrogels incorporating polymeric cell-adhesive peptide to promote the 3D assembly of tumoroids, Biomacromolecules 17 (2016) 3750–3760, https://doi.org/10.1021/acs.biomac.6b01266.

[78] V. Vassallo, C. Di Meo, N. Alessio, A. La Gatta, G.A. Ferraro, G.F. Nicoletti, C. Schiraldi, Highly concentrated stabilized hybrid complexes of hyaluronic acid: rheological and biological assessment of compatibility with adipose tissue and derived stromal cells towards regenerative medicine, Int. J. Mol. Sci. 25 (2024) 2019, https://doi.org/10.3390/ijms25042019.

[79] D. Tews, R.E. Brenner, R. Siebert, K.M. Debatin, P. Fischer-Posovszky, M. Wabitsch, 20 Years with SGBS cells - a versatile in vitro model of human adipocyte biology, Int. J. Obes. 46 (2022) 1939–1947.

[80] P.L. Nguyen, S.M.H. Alibhai, S. Basaria, A.V. D'Amico, P.W. Kantoff, N.L. Keating, D.F. Penson, D.J. Rosario, B. Tombal, M.R. Smith, Adverse effects of androgen deprivation therapy and strategies to mitigate them, Eur. Urol. 67 (2015) 825–836.

[81] P.I. Croucher, M.M. McDonald, T.J. Martin, Bone metastasis: the importance of the neighbourhood, Nat. Rev. Cancer 16 (2016) 373–386, https://doi.org/10.1038/nrc.2016.44.

[82] S. Horenburg, P. Fischer-Posovszky, K.M. Debatin, M. Wabitsch, Influence of sex hormones on adiponectin expression in human adipocytes, Horm. Metab. Res. 40 (2008) 779–786, https://doi.org/10.1055/s-0028-1083780.

[83] K.J. McInnes, K.A. Brown, N.I. Hunger, E.R. Simpson, Regulation of LKB1 expression by sex hormones in adipocytes, Int. J. Obes. 36 (2012) 982–985, https://doi.org/10.1038/ijo.2011.172.

[84] K.B. Singh, X. Ji, S.V. Singh, Therapeutic potential of leelamine, a novel inhibitor of androgen receptor and castration-resistant prostate cancer, Mol. Cancer Ther. 17 (2018) 2079–2090, https://doi.org/10.1158/1535-7163.MCT-18-0117.

[85] K.M. Wadosky, S. Koochekpour, Androgen receptor splice variants and prostate cancer: from bench to bedside, Oncotarget 8 (2017) 18550–18576, https://doi.org/10.18632/ONCOTARGET.14537.

[86] E.V. Morris, C.M. Edwards, The role of bone marrow adipocytes in bone metastasis, J. Bone Oncol 5 (2016) 121–123, https://doi.org/10.1016/j.jbo.2016.03.006.

[87] M. Onuma, J.D. Bub, T.L. Rummel, Y. Iwamoto, Prostate Cancer Cell-Adipocyte Interaction: leptin mediates androgen-independent prostate cancer cell proliferation through c-Jun NH 2-terminal kinase, J. Biol. Chem. 278 (2003) 42660–42667, https://doi.org/10.1074/jbc.M304984200.

[88] J.D. Bub, T. Miyazaki, Y. Iwamoto, Adiponectin as a growth inhibitor in prostate cancer cells, Biochem. Biophys. Res. Commun. 340 (2006) 1158–1166, https://doi.org/10.1016/j.bbrc.2005.12.103.

[89] S. Su, J. Cao, X. Meng, R. Liu, A. Vander Ark, E. Woodford, R. Zhang, I. Stiver, X. Zhang, Z.B. Madaj, et al., Enzalutamide-induced and PTH1R-mediated TGFBR2 degradation in osteoblasts confers resistance in prostate cancer bone metastases, Cancer Lett. 525 (2022) 170–178, https://doi.org/10.1016/j.canlet.2021.10.042.

[90] M.J. Wilson, R. Haller, S.Y. Li, J.W. Slaton, A.A. Sinha, N.F. Wasserman, Elevation of dipeptidylpeptidase IV activities in the prostate peripheral zone and prostatic secretions of men with prostate cancer: possible prostate cancer disease marker, J. Urol. 174 (2005) 1124–1128, https://doi.org/10.1097/01.ju.0000168621.84017.5c.

[91] K. Pan, W.P. Skelton, M. Elzeneini, T.-C. Nguyen, A.J. Franke, A. Ali, R. Bishnoi, L. Dang, N.H. Dang, J. Kish, A multi-center retrospective analysis examining the effect of dipeptidyl peptidase-4 inhibitors on progression-free survival in patients with prostate cancer, Cureus 13 (2021), https://doi.org/10.7759/cureus.14712.